

17. HYDROTHERMAL CONVECTION, REACTION, AND DIFFUSION IN SEDIMENTS ON THE COSTA RICA RIFT FLANK: PORE-WATER EVIDENCE FROM ODP SITES 677 AND 678¹

Michael J. Mottl²

ABSTRACT

Sites 677 and 678 were drilled on ODP Leg 111 to test hypotheses about the nature and pattern of hydrothermal circulation on a mid-ocean ridge flank. Together with earlier results from DSDP Site 501/504 and several heatflow and piston coring surveys covering a 100-km² area surrounding the three drill sites, they confirm that hydrothermal circulation persists in this 5.9-m.y.-old crust, both in basement and through the overlying sediments (Langseth et al., 1988).

Profiles of sediment pore-water composition with depth at the three drill sites show both vertical and horizontal gradients. The shapes of the profiles and their variation from one site to another result from a combination of vertical and horizontal diffusion, convection, and reaction in the sediments and basement. Chemical species that are highly reactive in the siliceous-calcareous biogenic sediments include bicarbonate (alkalinity), ammonium, sulfate, manganese, calcium, strontium, lithium, silica, and possibly potassium. Reactions include bacterial sulfate reduction, mobilization of Mn²⁺, precipitation of CaCO₃, and recrystallization of calcareous and siliceous oozes to chalk, limestone, and chert. Species with profiles more affected by reaction in basaltic basement than in the sediments include Mg, Ca, Na, K, and oxygen isotopes. Reaction in basement at 60°C and at higher temperatures has produced a highly altered basement formation water that is uniform in composition over distances of several kilometers. As inferred from the composition of the basal sediment pore water at the three sites, this uniformity extends from upflow zone to downflow zone in basement and the sediments. It exists in spite of large variations in heat flow and depth to basement, apparently as a result of homogenization by hydrothermal circulation in basement.

Profiles for chlorinity, Na, Mg, and other species in the sediment pore waters confirm that Site 678, drilled on a localized heatflow high identified by Langseth et al. (1988), is a site of long-lived upwelling of warm water from basement through the sediments at velocities of 1 to 2 mm/yr. The upflow through the anomalously thin sediments is apparently localized above an uplifted fault block in basement. This site and other similar sites in the survey area give rise to lateral diffusion and possibly flow through the sediments, which produces lateral gradients in sediment pore-water composition at sites such as 501/504. The complementary pore-water profiles at the low-heatflow Site 677 2 km to the south indicate that downflow is occurring through the sediments there, at comparable rates of 1 to 2 mm/yr.

INTRODUCTION

Since 1978, more than 300 heatflow measurements, 25 piston cores, eight boreholes, and several seismic-reflection lines have been made over a 100-km² area surrounding Deep Sea Drilling Project (DSDP) Site 501/504. A major objective of these studies has been to determine the nature and pattern of hydrothermal circulation on a mid-ocean ridge flank, the southern flank of the Costa Rica Rift. Sites 677 and 678 were drilled on Ocean Drilling Program (ODP) Leg 111 to test hypotheses of seawater circulation through the sediments and basement at this site.

DSDP Site 501/504 lies on 5.9-m.y.-old crust. Sediments in the area are continuous and generally 250 to 300 m thick. The mean conductive heat flow measured is 216 mW/m² (Langseth et al., 1988), close to the theoretically predicted value for cooling lithosphere of this age, indicating that advective heat loss through the sediment section is negligible. Heat flow is not uniform, however, but varies by $\pm 20\%$ about the mean in broad undulations that run east-west parallel to topography and the ridge axis to the north (Fig. 1). The wavelength of the undulations is 5 to 8 km. These broad heatflow variations are believed to result from hydrothermal circulation in basement.

Within the east-west bands of high heat flow are several small "warm spots" where heat flow exceeds 250 to 350 mW/m², to a measured maximum of 391 mW/m². Within these warm

spots, Langseth et al. (1988) found large vertical and horizontal gradients in the composition of the sediment pore waters, to a depth of 6 to 17 m below seafloor (mbsf), as sampled by piston coring. These gradients correlate closely with heat flow. The thermal and chemical anomalies that characterize the warm spots are narrow and elongate, ranging from 0.5 to 2 km north to south and 0.5 to 4 km east to west (Fig. 1). These observations strongly suggest that the anomalies are maintained by localized seepage of warm, altered seawater upward from basement through the sediment section. The convex-upward curvature of the pore-water chemical profiles suggests flow velocities of a few millimeters per year, as calculated from a one-dimensional advection-diffusion model by Langseth et al. (1988). This rate is sufficiently slow to be consistent with the linear temperature gradients measured in the shallow sediments.

Mottl et al. (1983) were the first to note that the composition of the sediment pore water varies laterally as well as vertically in this area. Five holes drilled within a total distance of 500 m at Site 501/504 on DSDP Legs 68 and 69 revealed lateral gradients comparable in size to the large vertical gradients. These lateral gradients did not extend high enough in the sediment section to be accessible to piston coring, however. Site 501/504 is located a few hundred meters northwest of the warm spot drilled as ODP Site 678, in an area where heat flow ranges from 6% to 28% above the regional average. Sediment thickness there ranges from 264 to 275 m, and water depth from 3458 to 3460 m.

Site 678 was targeted on a warm spot that had been defined by three piston cores and many heatflow measurements. Hole 678B was drilled within 200 m of the highest value found in this warm spot, 327 mW/m². The hole is 1.3 km southeast of Hole 504 and sits on a small hill that rises 20 to 30 m above the sur-

¹ Becker, K., Sakai, H., et al., 1989. *Proc. ODP, Sci. Results*, 111: College Station, TX (Ocean Drilling Program).

² Department of Oceanography and Hawaii Institute of Geophysics, University of Hawaii, Honolulu, HI 96822.

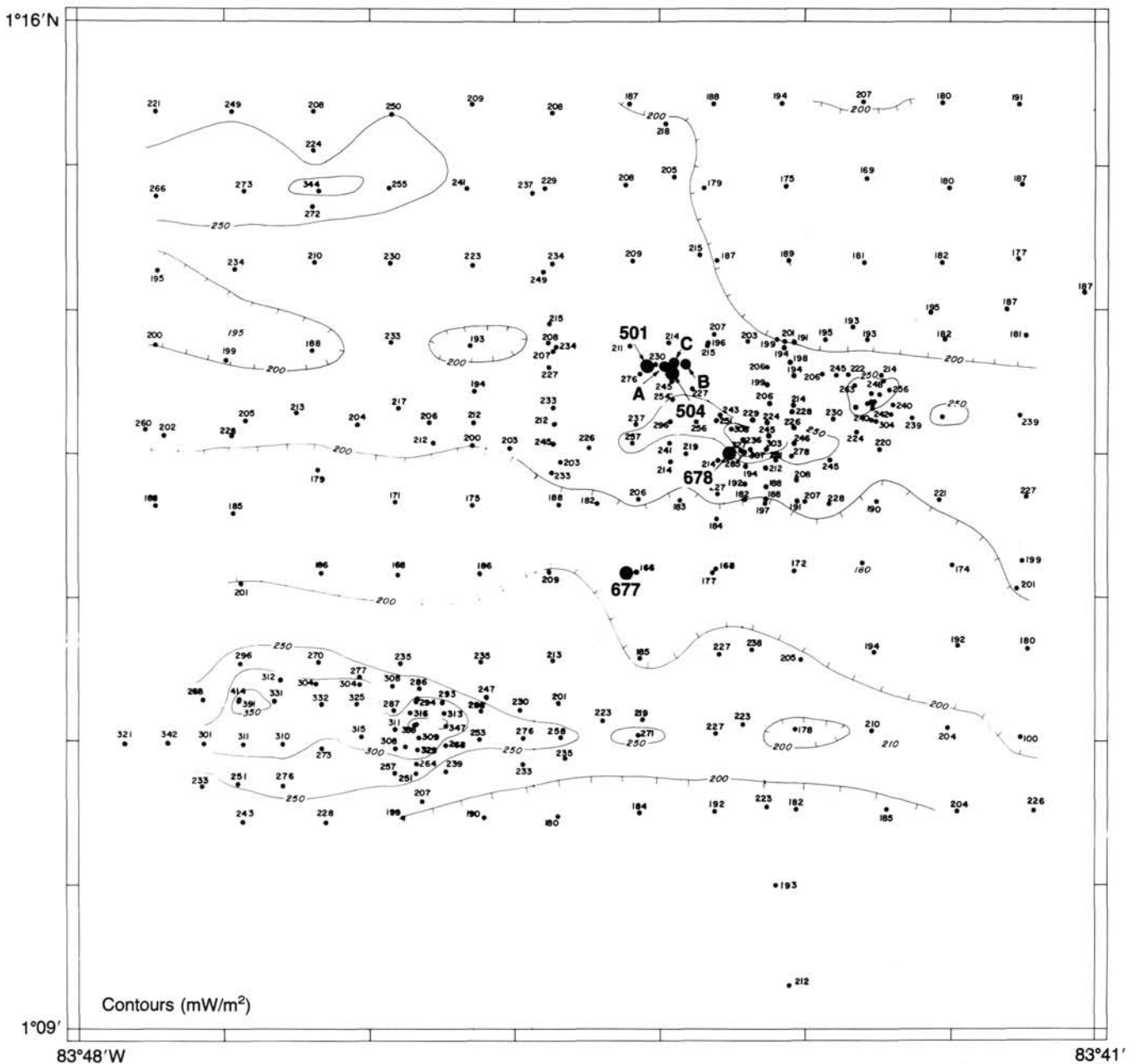


Figure 1. Locations of drill holes at DSDP Site 501/504 and ODP Sites 677 and 678, on a map of heatflow contours from Langseth et al. (1988).

rounding seafloor. This hill appears to be part of a discontinuous ridge that runs along the axis of a 4-km-wide east-west-trending trough. Basaltic basement was encountered at a depth of 171.8 mbsf. Water depth is 3445 ± 9 m.

ODP Site 677, by contrast, was targeted at the lowest heatflow value found in the entire 100-km²-survey area, 166 mW/m². Holes 677A and 677B are "zero-offset" holes drilled within a few tens of meters of each other near the center of the band of low heat flow which lies to the south of Sites 501/504 and 678 (Fig. 1). The holes are located on the southern edge of the aforementioned topographic trough, 2.6 km south-southwest of Hole 504 and 2.0 km southwest of Site 678. Basement was encountered at 309.4 mbsf. Water depth is 3461 m.

Major objectives at Sites 677 and 678 were (1) to test further the hypothesis that warm, altered seawater is seeping upward from basement through the sediments at rates of a few millime-

ters per year in a small area at Site 678, (2) to identify the factors that localize the upflow, (3) to determine whether the low heatflow areas such as that surrounding Site 677 represent complementary downflow zones, and (4) to determine whether the composition of formation water in the shallow basement, as reflected in the composition of the basal sediment pore water, varies laterally across the region from areas of high to low heat flow.

PROCEDURES

Sediment pore-water samples were obtained both by squeezing and, for two samples from Hole 677A only, with the Barnes *in-situ* sampler. Details of these procedures are given in the *Initial Reports* (Shipboard Scientific Party, 1988b). Sediments were squeezed at as close to *in-situ* temperature as possible, using previous temperature measurements in the area as a guide. No attempt was made to squeeze at higher than

room temperature, however. Temperature of squeezing approximated the estimated *in-situ* temperatures for samples from the upper 100 to 150 m of the sediment section, as shown in Figure 2.

All samples were filtered through 0.22- μ m Millipore cellulose acetate filters and analyzed in the laboratory aboard ship for pH; for chlorinity, alkalinity, Ca, and Mg by standard titration techniques; and for Si, ammonium, phosphate, and nitrate by colorimetry. Detailed methods and results are given in the *Initial Reports* (Shipboard Scientific Party, 1988b); results for some of these species are repeated in Table 1. Results for other species in Table 1 were determined at the University of Hawaii: sulfate by ion chromatography; K and Li by flame atomic absorption spectrophotometry (FAAS); Sr, Ba, Fe, and Mn by inductively-coupled plasma emission spectrometry (ICPES); and Na by charge balance. Aliquots for shorebased analysis were stored in sealed polyethylene tubes prior to analysis. Samples for determination of Sr, Ba, Fe, and Mn were also acidified to pH 2 with HCl. Determinations of Ca and Mg were repeated onshore, by both FAAS on unacidified aliquots and ICPES on acidified aliquots. Results are indistinguishable from those of the shipboard titrations. Because the titration data are much more precise they have been used in the figures presented here.

As noted in Table 1, the compositions reported for six samples were corrected to a constant chlorinity to account for evaporation or dilution that apparently occurred during core handling. These samples were recovered from near the basement interface and include chalk, limestone, and clay containing basalt fragments. Five of the six samples were taken

from the core catcher after the core was split. Because of their hardness and small size, the five core-catcher samples yielded only 1 to 7 mL of pore water each; the sixth sample yielded 13 mL.

Note that Hole 678B was washed without coring for most of its length due to time limitations; that is, penetration was achieved by washing the sediment away with a high-pressure stream of water. Core 111-678B-4W is a wash core collected from somewhere within a 65-m interval washed with a core barrel in place. This core was nonetheless subsampled for pore water because it inadvertently penetrated upper Miocene basaltic basement, which was encountered at a much shallower depth than expected. The upper three pore-water samples from this core have here been assigned arbitrarily to the midpoint depth of the washed interval, at about 139 mbsf, whereas the lower four samples from the core catcher have been assigned to the bottom of the interval because they are hard and contain chalk, limestone, clay, and basalt fragments.

RESULTS

The profiles of Ca and Mg vs. depth are mirror images of one another (Fig. 3). There is a marked contrast between the low-heatflow Site 677, where the profiles are convex downward, and the high-heatflow Site 678, where the profiles are convex upward. The largest vertical gradients occur within 20 m of basement for Site 677 and within 20 m of the seafloor for Site 678. The concentrations of both elements diverge near the seafloor and then converge again near basement, achieving nearly identical values at the two sites. The data from Sites 677 and 678, collected at extremes in heat flow for the area, bracket the data from Site 501/504, in spite of the large range in concentrations found at the latter site.

The Ca data for the lowermost six samples from Hole 678B scatter greatly, even after the correction for variable chlorinity made necessary by the problems with handling these very small samples taken from the core catcher. Most of the values, along with that for the lowermost sample from Hole 677A, also from the core catcher, are anomalously high. The concentration of dissolved Ca in these samples exceeds that higher in the section, but it does not increase monotonically with depth as basement is approached. Rather, the data are scattered (Table 1). Moreover, the apparent increase in Ca is not accompanied by a decrease in Mg; the lowermost samples from both holes show much less variation in Mg. Charge-balance constraints indicate that the apparent increase in Ca is accompanied by an equivalent decrease in Na. It is possible that this exchange of Na for Ca is an artifact of sample recovery which resulted from ion exchange between the pore waters and these small, semilithified, clay-rich samples because of a decrease in the temperature and pressure from *in-situ* conditions. Gieskes (1983) has observed a similar exchange of Na for Ca in Mg-depleted pore waters squeezed from clay layers interbedded with basalts in several DSDP holes; these changes may similarly be artifacts of sample recovery.

The depth profiles for Sr and Ba (Fig. 4) resemble that for Ca, except that the Sr concentrations at Site 501/504 exceed those at Site 678. There is a large squeezing artifact for Ba: the two *in-situ* samples from Hole 677A have about twice as much Ba as the squeezed samples from similar depths. There are no Ba data available for Site 501/504.

The profile for sulfate (Fig. 5A) resembles that for Mg. Both species decrease greatly with depth but level off at a concentration well above zero. The profile for Mn (Fig. 5B) is similar at all three sites, increasing rapidly to high concentrations near the seafloor and then decreasing to low concentrations at depth.

The profiles for alkalinity and ammonium (Fig. 6) both exhibit maxima at shallow to middle depths in the sedimentary section. Alkalinity decreases to low values near basement in all holes.

The profile for K (Fig. 7A) resembles that for Mg: Site 677 generally has the highest concentrations at a given depth and

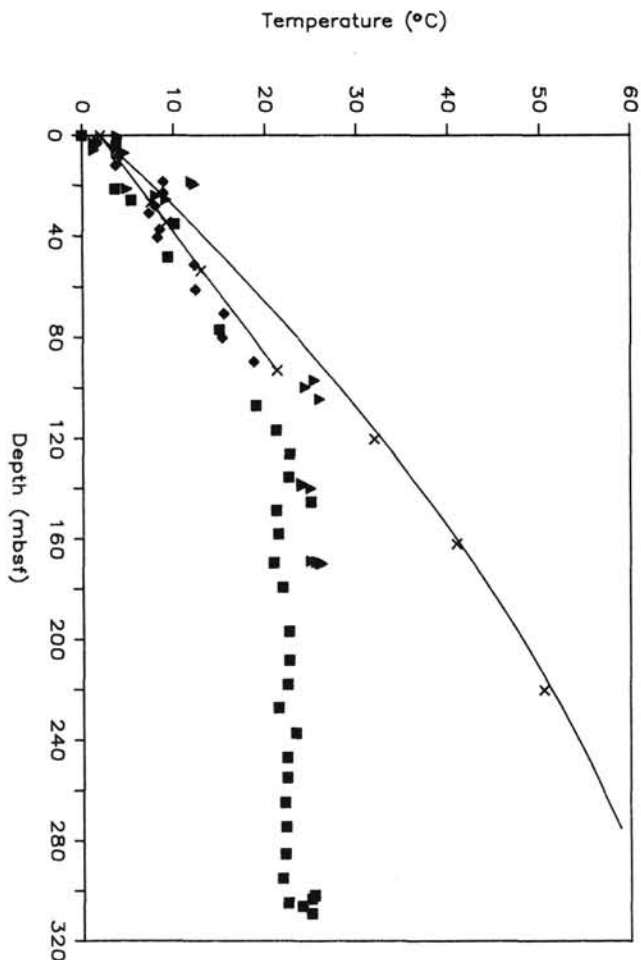


Figure 2. Temperature of squeezing for sediment pore-water samples from Holes 677A (squares), 677B (diamonds), and 678B (triangles), compared with *in-situ* temperatures (X's) measured in Holes 501 and 504C to 220 mbsf (upper curve: $T = -0.00032d^2 + 0.295d + 2$) and Holes 677A and 677B to 93 mbsf (lower line: $T = 0.208d + 2.01$).

Table 1. Composition of sediment pore waters from ODP Sites 677 and 678.

Sample no. ^a	Core, section, interval (cm) ^b	Depth (mbsf)	Volume (mL)	Chlorinity (mmol/kg)	Sulfate (mmol/kg)	Alkalinity (mmol/kg)	Na ⁺ (mmol/kg)	K ⁺ (mmol/kg)	Li ⁺ (μmol/kg)	Ca ²⁺ (mmol/kg)	Mg ²⁺ (mmol/kg)	Sr ²⁺ (μmol/kg)	Ba ²⁺ (μmol/kg)	Fe ²⁺ (μmol/kg)	Mn ²⁺ (μmol/kg)	Si (μmol/kg)	Na/Cl (mol/mol)	
Surface seawater (9 October 1986)				519.2	27.0		(446.4)	9.90	25.5	9.67	49.88	85.3	0.02					(0.8598)
Bottom seawater (Cruise TT198, May 1986)				540.9	27.0	2.44	463.5	10.07	26.1	10.19	52.63	88.2	0.14			161	0.8569	
111-677A-																		
IW1	1H-3, 145-150	4.5	102	542.6	28.2	2.93	465.1	12.15	28.2	10.12	51.88	91.5	0.32	45.4	130.3	646	0.8571	
IW2	2H-1, 80-89	7.0	48	541.6	28.3	3.49	461.7	13.35	29.8	9.71	53.31	91.2	0.35	5.9	79.4	781	0.8524	
IW3	3H-4, 120-125	21.4	95	545.4	28.1	3.89	466.4	12.72	29.0	9.47	53.36	90.5	0.30		79.4	693	0.8551	
IW4	4H-1, 55-74	25.8	34	547.3	27.8	4.28	469.7	12.20	28.0	9.42	52.93	92.2	0.32	10.6	73.1	868	0.8582	
IW5	5H-1, 51-69	35.3	35	548.7	27.9	4.35	471.0	12.06	27.9	9.54	53.05	92.4	0.42	5.4	79.4	1014	0.8584	
IW6	6H-3, 120-125	48.4	88	553.8	27.8	4.21	474.4	12.02	27.9	9.62	53.60	93.2	0.33		65.3	847	0.8566	
IW7	9H-3, 120-125	76.9	93	557.6	27.0	5.79	477.7	11.36	24.5	10.34	53.43	96.3	0.36	3.2	47.7	1095	0.8568	
IW8	12H-4, 120-125	106.9	101	556.2	26.8	3.98	474.9	10.98	27.7	10.08	53.54	91.8	0.35		40.4	1236	0.8539	
IW9	13H-4, 145-150	116.7	99	555.7	26.8	4.99	476.1	10.69	24.3	10.51	52.79	98.9	0.36	7.7	13.6	1379	0.8568	
IW10	14H-4, 145-150	126.2	102	548.2	27.1	4.93	470.1	10.49	23.1	11.77	51.14	104	0.40	17.0	9.4	1412	0.8576	
IW11	15H-4, 120-125	135.4	93	550.1	27.0	4.92	470.3	10.24	23.6	13.78	50.90	111	0.35	5.5	7.0	1466	0.8550	
IW12	16X-4, 145-150	145.2	45	550.1	26.5	4.51	470.7	10.05	23.9	14.63	48.42	113	0.35	2.4	4.5	1296	0.8556	
IW13	17X-3, 145-150	148.7	47	546.3	25.7	4.60	464.9	9.91	23.9	16.01	47.32	121	0.32	3.5	4.0	1471	0.8510	
IW14	18X-3, 120-125	158.0	89	542.6	25.6	4.84	461.8	9.62	23.1	16.65	46.55	123	0.29	1.8	3.4	1388	0.8513	
BW15	B	163.6	20	544.4	26.8	6.14	465.2	10.88	23.4	18.83	44.82	131	0.67	45.8	11.1	1815	0.8545	
*15ov.		163.6	1168	499.3	26.9			0.09	26.8	18.71	45.15	134	0.66	0.0	8.6	1739		
IW16	19X-4, 145-150	169.5	84	545.4	26.0	3.99	465.4	9.60	23.6	17.74	45.12	126	0.31	2.3	3.9	1417	0.8534	
IW17	20X-4, 145-150	179.2	81	549.1	26.0	5.15	469.6	10.06	24.3	19.23	43.70	137	0.33	1.3	3.4	1649	0.8551	
IW18	22X-3, 120-125	196.6	67	545.4	26.1	4.88	467.0	9.68	24.5	19.36	43.22	137	0.35	3.3	2.0	1658	0.8562	
IW19	23X-4, 145-150	208.1	57	546.3	25.5	4.46	467.3	9.64	22.7	19.92	42.15	140	0.32	1.5	2.3	1761	0.8554	
BW20	B	211.8	18	541.6	27.4	4.69	463.0	9.84	25.5	19.04	44.69	138	0.55	14.4	4.0	2015	0.8547	
*20ov.		211.8	760	478.6	25.8			9.43	29.9	19.58	43.88	144	0.69	6.6	5.3	2163		
IW21	24X-4, 145-150	217.7	91	547.4	25.7	4.88	468.3	9.84	23.1	19.72	42.62	154	0.43	0.2	2.9	699	0.8555	
IW22	25X-4, 120-125	227.1	68	552.1	26.7	2.74	473.4	9.53	24.5	19.62	42.72	140	0.36	1.7	1.9	1629	0.8575	
IW23	26X-4, 145-150	237.1	67	553.1	25.7	4.46	473.5	9.48	24.1	20.95	41.55	155	0.41	0.4	2.4	1782	0.8562	
IW24	27X-4, 145-150	246.8	70	549.3	26.2	4.36	470.7	9.42	32.9	21.40	41.10	152	0.39	8.5	2.6	1791	0.8570	
IW25	28X-3, 120-125	254.6	67	549.3	26.1	3.61	471.1	9.24	24.5	21.64	40.31	158	0.32	1.0	2.5	1791	0.8577	
IW26	29X-3, 145-150	264.5	55	546.5	25.5	3.43	467.2	8.66	24.8	22.19	40.00	158	0.35	0.6	2.3	1649	0.8548	
IW27	30X-3, 145-150	274.2	45	551.2	27.1	4.03	473.6	8.94	23.6	23.10	39.95	160	0.38	2.7	2.8	1753	0.8592	
IW28	31X-4, 120-125	285.0	55	548.4	25.7	2.83	466.8	8.37	24.2	24.27	39.01	162	0.34	0.9	3.2	1750	0.8513	
IW29	32X-4, 145-150	294.9	55	550.2	25.2	2.80	467.7	8.47	24.5	28.00	35.24	179	0.37	1.9	4.2	1805	0.8500	
IW31	33X-2, 145-150	301.6	74	545.1	24.4	2.30	460.8	8.44	24.1	31.38	31.70	177	0.37		5.3	1525	0.8453	
IW34	33X-3, 133-150	303.0	54	554.9	24.9	1.22	470.0	8.87	25.3	30.53	32.53	184	0.38	2.4	5.4	1354	0.8469	
IW30	33X-4, 145-150	304.6	49	544.1	21.2	0.37	457.5	6.26	20.3	48.11	13.08	229	0.56	1.2	8.8	686	0.8408	
*IW32	33X-5, 123-140	305.9	13	571.8	21.8	0.34	460.4	6.09	17.6	52.30	11.02	252	0.45	7.5	8.7	345	0.8371	
*IW33	34X-CC, 23-31	308.9	1	510.9	22.0		(429.5)	6.82	86.2	68.63	9.94	247			14.5	399	(0.7809)	
Basement		309.4																
111-677B-																		
IW1	1H-1, 95-100	1.0	98	540.7	28.1	2.88	465.4	11.79	27.4	9.92	51.11	91.1	0.28	4.1	79.1	544	0.8608	
IW2	1H-2, 145-150	3.0	88	538.8	27.8	3.08	462.8	12.31	29.0	9.86	51.09	91.7	0.25	3.9	64.6	640	0.8589	
IW3	2H-1, 145-150	9.1	95	538.8	27.8	3.58	462.8	12.22	24.8	9.85	51.34	93.2	0.28	4.3	84.9	702	0.8589	
IW4	2H-3, 145-150	12.1	88	539.7	27.3	3.45	462.4	12.24	24.8	9.41	51.85	93.7	0.29	3.9	68.8	698	0.8566	
IW5	3H-1, 145-150	18.6	77	545.2	27.3	3.74	467.7	12.38	25.3	9.28	52.08	91.2	0.29	5.8	64.5	723	0.8580	
IW6	3H-4, 145-150	23.1	77	545.2	27.3	4.45	468.6	12.20	24.8	9.38	51.97	94.6	0.33	5.2	75.3	750	0.8596	
IW7	4H-1, 145-150	28.1	84	545.2	27.3	4.18	467.9	12.17	25.1	9.51	52.14	89.8	0.29	3.7	68.4	793	0.8584	
IW8	4H-3, 145-150	31.1	90	548.9	27.0	4.16	471.3	11.79	24.5	9.53	52.13	90.9	0.25	4.1	76.7	798	0.8586	
IW9	5H-1, 145-150	37.6	48	546.5	27.1	3.85	467.9	12.34	27.4	9.49	52.32	91.8	0.32	24.1	67.6	823	0.8561	
IW10	5H-3, 145-150	40.6	74	557.4	27.9	4.35	478.0	11.74	26.2	9.85	53.77	93.9	0.28	4.4	64.0	783	0.8575	
IW11	6H-4, 120-125	51.3	74	554.6	27.5	4.00	475.4	12.02	25.7	9.62	53.16	92.3	0.28	3.9	49.7	857	0.8572	
IW12	7H-4, 145-150	61.1	91	553.6	27.6	4.61	475.1	11.43	26.2	10.15	52.92	94.8	0.32	4.7	54.2	920	0.8581	
IW13	8H-4, 145-150	70.6	94	553.6	26.2	5.03	472.5	11.63	25.4	10.32	52.75	99.8	0.31	5.8	49.6	958	0.8534	
IW14	9H-4, 145-150	80.1	105	549.9	26.8	5.43	470.1	11.36	24.4	10.30	53.08	100.5	0.32	5.5	47.0	1016	0.8549	
IW15	10H-4, 145-150	89.6	91	545.2	26.8	5.38	466.6	11.27	22.9	10.22	52.57	99.8	0.35	4.3	35.9	1034	0.8559	

Table 1 (continued)

Sample no. ^a	Core, section, interval (cm) ^b	Depth (mbsf)	Volume (mL)	Chlorinity (mmol/kg)	Sulfate (mmol/kg)	Alkalinity (mmol/kg)	Na ⁺ (mmol/kg)	K ⁺ (mmol/kg)	Li ⁺ (μmol/kg)	Ca ²⁺ (mmol/kg)	Mg ²⁺ (mmol/kg)	Sr ²⁺ (μmol/kg)	Ba ²⁺ (μmol/kg)	Fe ²⁺ (μmol/kg)	Mn ²⁺ (μmol/kg)	Si (μmol/kg)	Na/Cl (mol/mol)	
Surface seawater (9 October 1986)				519.2	27.0		(446.4)	9.90	25.5	9.67	49.88	85.3	0.02					(0.8598)
Bottom seawater (Cruise TT198, May 1986)				540.9	27.9	2.44	463.5	10.07	26.1	10.19	52.63	88.2	0.14			161	0.8569	
111-678B-																		
IW1	1H-1, 45-50	0.5	86	544.1	27.5	2.52	468.0	11.78	28.7	11.86	48.78	110	0.50	6.5	101.0	530	0.8602	
IW2	1H-1, 145-150	1.5	99	541.3	27.0	2.66	465.7	11.70	28.9	13.57	46.44	124	0.52	5.6	85.4	592	0.8604	
IW3	1H-2, 145-150	3.0	107	540.4	25.4	2.41	462.6	11.76	29.4	17.05	42.25	157	0.49	5.4	66.5	648	0.8561	
IW4	1H-4, 145-150	6.0	89	539.4	20.5	1.66	458.4	11.02	28.9	33.00	22.76	286	0.47	4.5	64.7	735	0.8499	
IW22	1H-5, 114-125	7.2	40	540.4	19.4	0.69	460.8	12.61	29.0	35.99	16.62	317	0.50	5.5	36.9	725	0.8528	
IW5	2H-1, 45-50	18.7	57	547.9	17.5	0.83	460.7	10.69	28.9	45.18	10.26	382	0.53	3.4	87.4	986	0.8408	
IW6	2H-1, 145-150	19.7	100	543.2	17.8	0.96	456.7	10.43	27.9	44.90	10.63	377	0.64	5.2	83.9	966	0.8407	
IW7	2H-2, 145-150	21.2	74	549.8	17.3	0.84	460.6	9.70	26.4	46.40	10.31	388	0.56	5.2	76.2	835	0.8378	
IW8	2H-4, 145-150	24.2	90	548.8	17.6	0.55	461.1	10.25	25.9	47.15	8.77	384	0.66	5.0	59.3	862	0.8402	
IW9	2H-5, 145-150	25.7	70	545.1	17.4	0.89	457.9	9.88	28.4	46.86	8.90	384	0.55	4.5	76.0	993	0.8401	
IW10	3H-1, 145-150	97.0	84	545.1	18.7	0.62	458.3	7.89	20.1	48.66	9.22	343	0.76	4.3	21.3	1475	0.8408	
IW11	3H-3, 120-125	99.7	74	547.3	17.8	1.12	459.4	7.71	20.9	50.43	7.45	348	0.94	3.4	20.9	1516	0.8395	
IW12	3H-6, 145-150	104.5	66	549.6	18.4	0.60	460.7	7.71	20.9	50.72	8.04	347	0.69	4.3	20.2	1498	0.8382	
IW13	4W-2, 55-67	138.0	36	546.1	21.3	0.75	461.8	7.73	20.6	43.49	15.99	295	0.63	5.0	16.5	1199	0.8456	
IW14	4W-3, 95-107	138.9	36	547.3	20.6	0.49	461.5	6.79	20.7	50.13	9.74	335	0.53	4.1	15.2	1504	0.8433	
IW15	4W-4, 145-150	139.9	75	546.3	16.9	0.68	453.9	6.99	20.0	50.77	8.71	324	0.94	3.6	14.3	1392	0.8309	
IW16	4W-CC, 3-15	168.9	26	546.3	23.4	0.58	463.2	6.65	18.4	44.85	16.68	262	0.55	4.8	15.9	447	0.8478	
*IW17	4W-CC, 18-25	169.0	6	539.0	23.3		(450.0)	6.39	17.4	55.22	14.57	298	1.19		21.6	145	(0.8182)	
*IW18	4W-CC, 30-42	169.2	7	525.8	22.8		(435.3)	6.55	15.4	63.85	12.73	333	1.40		14.3	152	(0.7914)	
IW19	4W-CC, 50-60	169.4	2	554.9	19.9		(435.8)	7.43	14.3	68.50	6.91	319				158	(0.7854)	
*IW20	5X-CC, 5-11	169.7	3	531.0	20.0		(435.8)	6.48	17.0	60.77	12.86	295			19.1	172	(0.7923)	
*IW21	5X-CC, 22-32	169.9	1.5	495.9	19.5		(427.1)	6.94	19.5	69.32	7.84	374			10.1	157	(0.7765)	
Basement		171.8																

Note: Chlorinity listed is as measured; concentrations of all other species in designated (*) samples have been corrected to a chlorinity of 550 mmol/kg in the table, or, for the Barnes overflow samples, to the chlorinity of the sample from the main coil. Values in parentheses were calculated assuming a value for alkalinity.

^a IW = squeezed; BW = Barnes *in-situ* sample; ov. = from overflow chamber of Barnes sampler, diluted with distilled water during sampling.

^b H = hydraulic piston core; X = extended barrel core; B = Barnes sample; W = wash core; CC = core catcher.

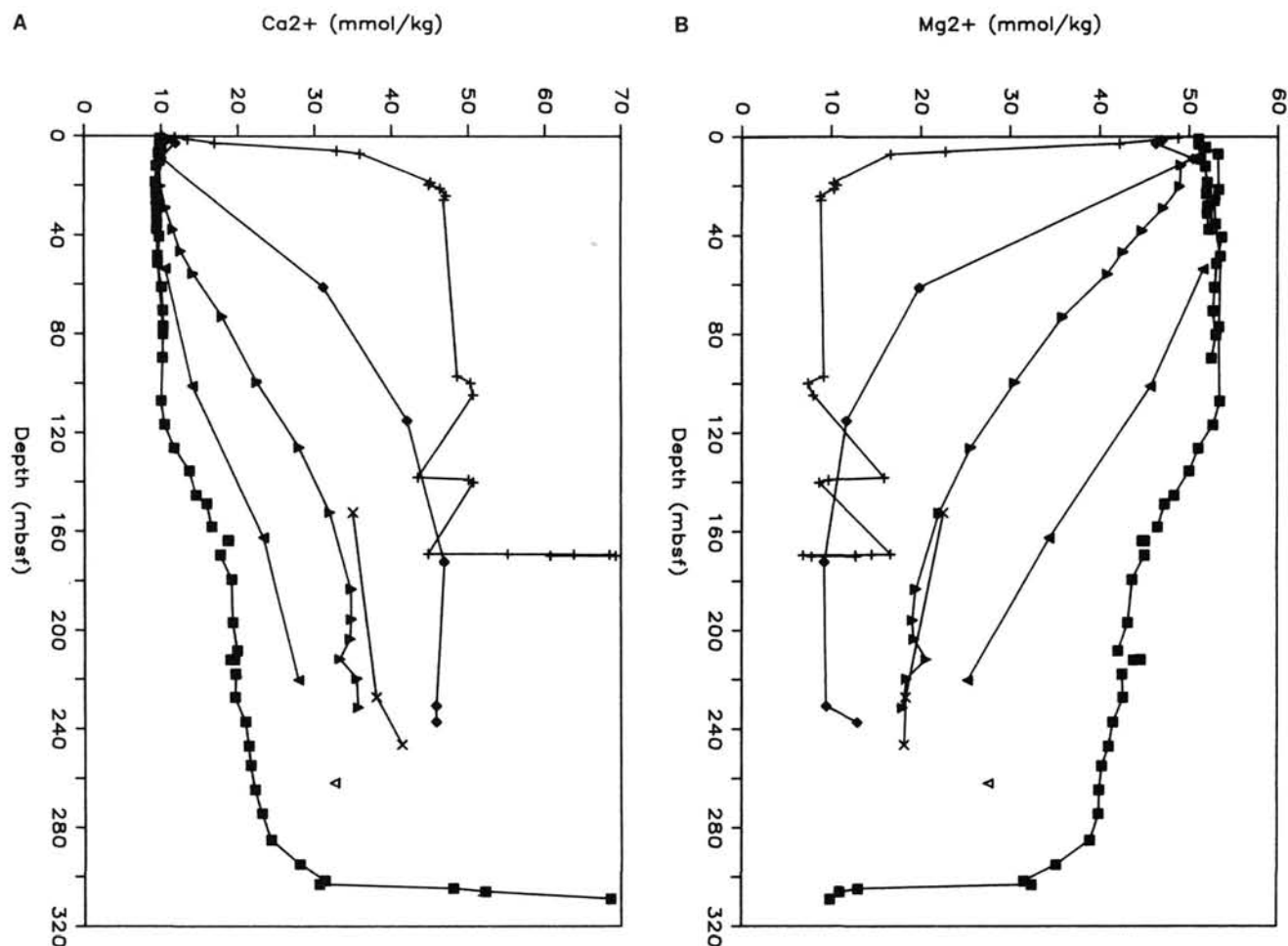


Figure 3. Concentrations of Ca^{2+} (A) and Mg^{2+} (B) in sediment pore waters from Holes 677A and 677B (squares), 678B (crosses), 501 (diamonds), 504 (triangles), 504A (X's), 504C (solid inverted triangles), and 504B (open inverted triangle).

has a convex-downward profile, whereas Site 678 has the lowest concentrations and a convex-upward profile. The enhancement by about 2 mmol/kg in the upper sediments probably results from a squeezing artifact; this artifact diminishes with depth as the *in-situ* temperature rises, causing a nearly linear decrease in K to the seawater value at a depth of about 160 mbsf. Below that depth K decreases more slowly until basement is approached, at which point it decreases rapidly along with Mg. The two *in-situ* samples from Hole 677A indicate that there is only a small squeezing artifact at 164 and 212 mbsf, despite an *in-situ* temperature that is probably much higher than the squeezing temperature (Fig. 2). The profile for Li (Fig. 7B) is largely similar to that for K at Sites 677 and 678, except for the single high basal value at Site 677. The Li profiles at Sites 677 and 678 do not display the midpoint depth maximum seen at Site 501/504.

The profile for Si (Fig. 8) is similar at all three sites, showing a gradual increase with depth followed by a sudden decrease, near basement for Sites 677 and 678 and at the diagenetic boundary between chalk and chert-limestone at Sites 677 and 501/504. Note that the two *in-situ* samples are 25% higher in Si content than their squeezed counterparts.

The profiles for chlorinity and Na (Fig. 9) are very similar to one another. Sites 677 and 501/504 show a 3% increase from bottom-water values to a maximum at 40 to 120 mbsf, followed by a 3% decrease to about 220 mbsf and a second increase below that. The deepest Hole 677A shows a second decrease as basement is approached, especially for Na. Site 678 apparently

has a different pattern; the increase in the shallow sediments is muted for chlorinity and nonexistent for Na, which decreases over the upper 20 m of the sediment section and then levels off.

Plotting the profile of the ratio of Na to chlorinity (Fig. 10) eliminates most of the erratic changes with depth. The Site 501/504 holes show a nearly linear decrease with depth, as noted by Mottl et al. (1983). Site 677 parallels this decrease to a depth of 160 mbsf, then increases slightly before decreasing precipitously near basement, in parallel with Na. Site 678 again is distinct from the other sites, showing a convex-upward profile that resembles that of Na, Mg, sulfate, alkalinity, and K.

DISCUSSION

The depth profiles for various species dissolved in the sediment pore waters result from three processes: reaction, diffusion, and convection. Reaction can occur within either the sediments themselves or the underlying basaltic basement. Diffusion and convection can occur laterally as well as vertically, as indicated by the large horizontal gradients in heat flow and sediment pore-water composition at these sites.

In order to understand the role of these processes, it is necessary to (1) characterize the chemical reactions in the sediments, (2) determine the composition of formation water in the shallow basement, (3) quantify the velocity (both speed and direction) of flow through the sediments, and (4) quantify the effects of diffusion. Ultimately, if the rates of convection and diffusion can be determined from the profile shapes of the relatively unre-

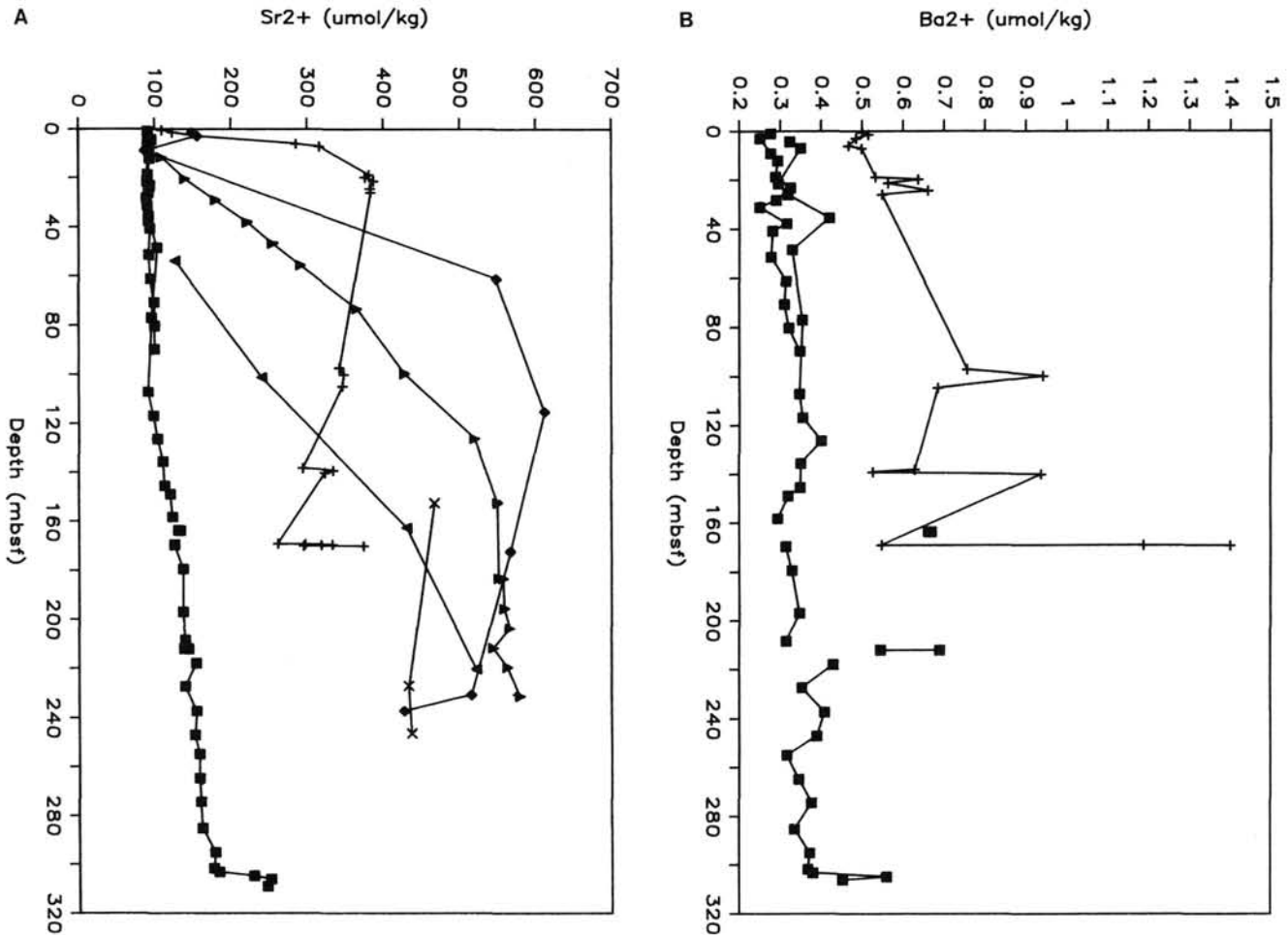


Figure 4. Concentration of Sr^{2+} (A) and Ba^{2+} (B) in sediment pore waters from Holes 677A, 677B, 678B, 501, 504, 504A, and 504C. Symbols are the same as in Figure 3. For Ba, the two *in-situ* samples from Hole 677A fall at higher concentrations than the squeezed samples from the same depths.

active species, it should be possible as well to infer the rates of various chemical reactions in the sediments from the profiles of appropriate reactants and products.

Reaction in the Sediments

Mottl et al. (1983) inferred the reactions that have affected the profiles at Site 501/504. The major reactions in the sediments are (1) bacterial reduction of seawater sulfate at depth, utilizing organic matter and producing alkalinity, ammonium, and H_2S ; (2) precipitation of CaCO_3 in response to the heightened alkalinity; (3) reduction of manganese oxides and diagenetic remobilization of Mn^{2+} ; (4) recrystallization of calcareous ooze to chalk and then limestone; and (5) recrystallization of opal-A in siliceous ooze to opal-CT and, ultimately, chert. All of these reactions occur at all three sites, except that chert has not been found at Site 678.

The depth to the diagenetic boundary between ooze and chalk varies inversely with the heat flow at the three sites, from 28 to 96 mbsf at Site 678 (the range results from incomplete coring at this site), to 144 mbsf at Site 501/504, to 154 to 183 mbsf at Site 677, where the transition is gradual. The deeper boundary between chalk and limestone varies in the same sense, from 112 to 169 mbsf at Site 678, to 227 to 234 mbsf at Site 501/504, to 303 mbsf at Site 677. At Sites 501/504 and 677, chert first appears at about the same depth as limestone.

The depth to these diagenetic boundaries presumably is a function of temperature. Temperatures measured in the sediments are shown in Figure 2. Site 501/504 appears to have a slightly higher thermal gradient than Site 677. Because the sediments are thinner there, however, the projected basement temperatures vary only slightly, from 58°C for Site 501/504 at 270 mbsf to about 66°C for Site 677 at 309.4 mbsf. The temperature estimate for Site 677 is based on a linear extrapolation over 216 m depth and is highly uncertain (Becker, this volume). No reliable temperatures were obtained at Site 678.

These reactions in the sediments can explain many characteristics of the pore-water profiles. Bacterial sulfate reduction must have produced much of the decrease in sulfate in the upper 100 m, considering the large increases in alkalinity and ammonium over the same interval. A similar decrease in sulfate, from 28 to 17 mmol/kg to a depth of 100 m, occurs in similar oozes 80 km to the north at DSDP Site 505, and there the decrease is unequivocally due to bacterial sulfate reduction (Mottl et al., 1983). The similarity of the sulfate profile (Fig. 5A) to that for Mg (Fig. 3B), however, suggests that reaction in basement has also contributed to the decrease in sulfate with depth, as subsequently discussed. The reducing nature of the sediments is responsible for the high concentrations of dissolved Mn in the surficial sediments.

Bacterial sulfate reduction produces 1 meq of alkalinity for each 1 meq of sulfate consumed. Except for the upper 140-m

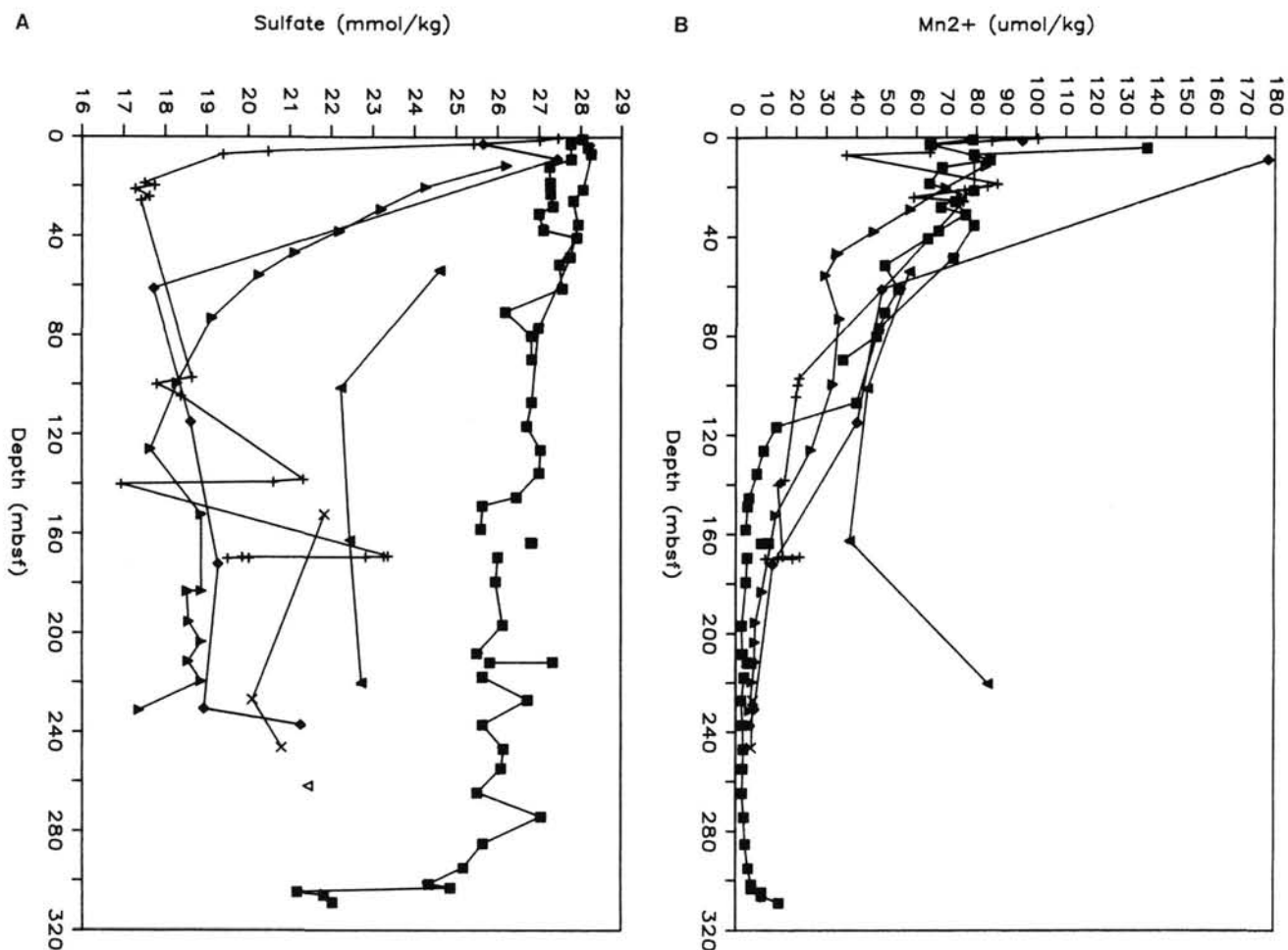


Figure 5. Concentrations of sulfate (A) and Mn^{2+} (B) in sediment pore waters from Holes 677A, 677B, 678B, 501, 504, 504A, 504C, and 504B. Symbols are the same as in Figure 3.

section at Site 677, the sulfate loss relative to bottom seawater greatly exceeds the alkalinity gain (Fig. 11B). Some of the alkalinity gain has almost certainly been lost subsequently by $CaCO_3$ precipitation, as was documented at Site 505. This loss is difficult to quantify at the present three sites, however, because Ca has increased there rather than decreased as it did at Site 505, and alkalinity has decreased below seawater values in the deeper samples.

That $CaCO_3$ precipitated in the sediments at Sites 678 and 501/504 is supported by the Ca-Mg relationships. The loss of Mg from the sediment pore waters relative to bottom seawater exceeds the gain of Ca at these two sites; at Site 677 the two are about equal (Fig. 11A). The difference between the sites is probably due to precipitation of $CaCO_3$ in the sediments. This conclusion is reinforced by a plot of Ca vs. Mg in the sediment pore waters (Fig. 12). Sites 678 and 501/504 exhibit nonlinear relationships between these elements at various depths throughout the sediments, indicating reaction. Site 677, by contrast, in which $CaCO_3$ precipitation is minimal based on sulfate-alkalinity and Ca-Mg relationships (Fig. 11), shows a linear relationship except for the small-volume samples from very near the basement interface. As noted previously, the large Ca variation in these latter samples is probably an artifact of sampling.

Another element that has almost certainly been affected by recrystallization of $CaCO_3$ in the sediments is Sr. Like other species reactive in the sediments, including alkalinity and ammonium, the concentrations of Sr at Site 501/504 fall outside the

bounds set by Sites 677 and 678. This phenomenon is also exhibited by Li, which probably varies as a result of recrystallization of silica. Dissolved silica increases with depth along with temperature throughout the ooze and chalk and then decreases abruptly where chert first appears at Sites 677 and 501/504 and within 3 m of basement at Site 678.

Potassium shows a large enrichment in the surficial sediments. Whether this enrichment is real or results from an irreversible temperature-of-squeezing artifact is not known, although the latter seems more likely.

In summary, the species that are highly reactive in the sediments are alkalinity, ammonium, sulfate, Mn, Ca, Sr, Li, Si, and possibly K.

Reaction in Basaltic Basement

A remarkable feature of the depth profiles is the tendency for the pore waters from all of the holes to approach the same composition near the basement interface. This tendency is shown by all 13 species plotted in Figures 3 through 9. The approximate composition of the basal sediment pore water is given in Table 2, along with the composition of waters sampled at various depths from the basement section of Hole 504B on DSDP Leg 83 and ODP Leg 111. All of these waters have gained Ca and Si and lost Mg, Na, K, sulfate, and alkalinity relative to bottom seawater. These directions of net transfer between basalt and seawater are similar to those observed in laboratory experi-

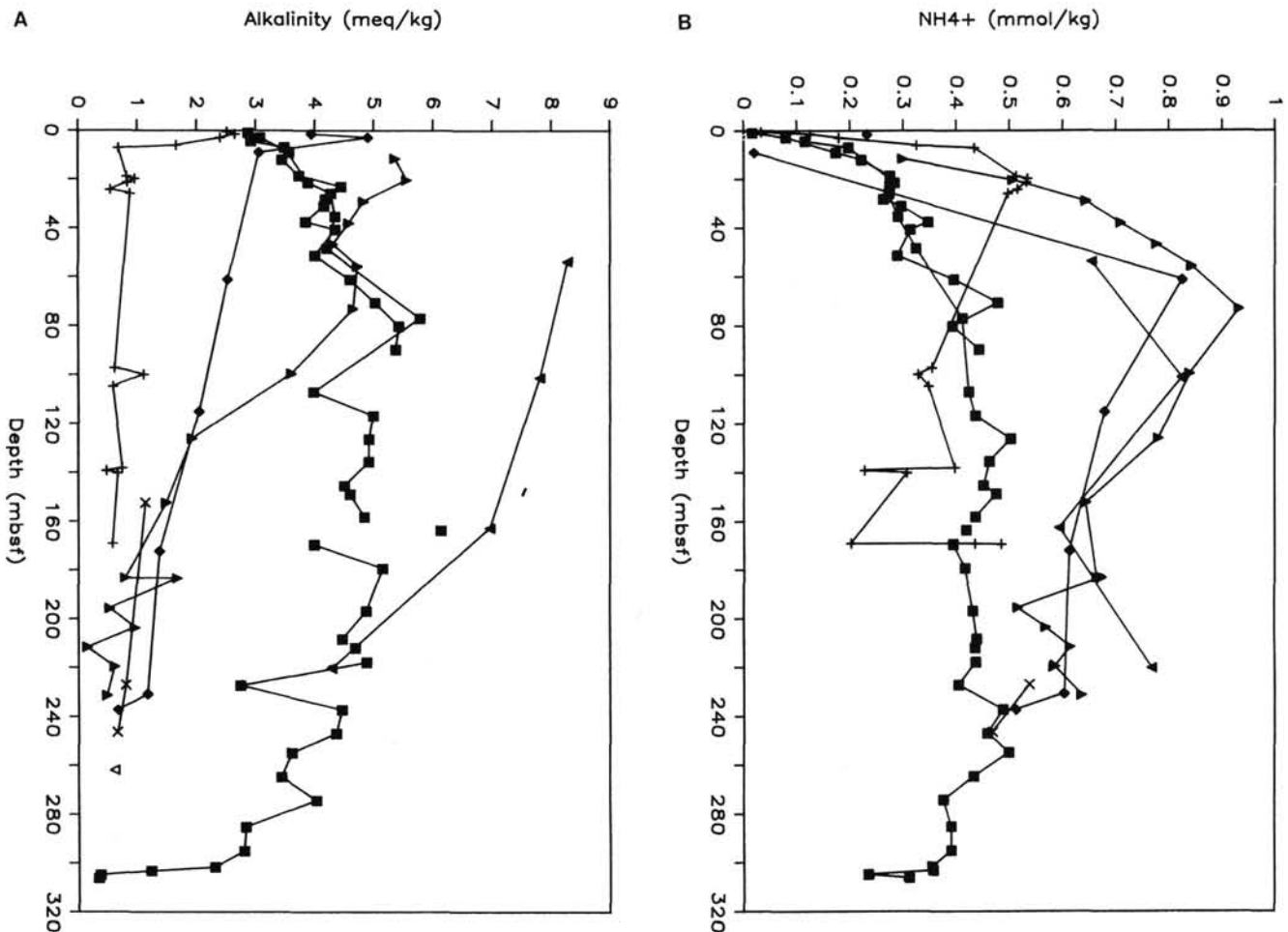


Figure 6. Concentrations of alkalinity (A) and ammonium (B) in sediment pore waters from Holes 677A, 677B, 678B, 501, 504, 504C, and 504B. Symbols are the same as in Figure 3.

ments at moderately elevated temperatures (Seyfried and Bischoff, 1979; Seyfried and Mottl, 1982).

Based on the accompanying ^{18}O depletion, Mottl et al. (1983) concluded that the Ca enrichment and Mg depletion in the sediment pore waters at Site 501/504 result from alteration of basaltic basement beneath the sediments. The constancy in composition of the basal sediment pore water at all three sites, in spite of the range in depth to basement from 172 to 309 mbsf, supports this conclusion. As noted previously, the temperature at the basement interface almost certainly varies proportionately less than the depth to basement, probably by less than 5° to 10°C . The composition of interstitial water in the upper basement is apparently also uniform from site to site.

This conclusion is consistent with that of Langseth et al. (1988) based on heatflow data, that hydrothermal circulation persists in the shallow basement at flow velocities of 10 to 30 cm/yr. Such velocities would be adequate to homogenize any small differences in formation-water composition that arose from basalt-seawater reaction at slightly different temperatures.

In summary, the species for which depth profiles are more affected by reaction in basement than in the sediments are Mg, Ca, Na, K, and oxygen isotopes.

Vertical Convection through the Sediments

Given that the vertical gradients in sediment pore-water composition arise mainly by reaction in the sediments and basement, it still remains to explain the lateral gradients. As noted

previously, Langseth et al. (1988) concluded that the large lateral gradients at Site 678 and two other "warm spots" are caused by upward seepage of warm, altered seawater from basement. The shapes of the depth profiles in Figures 3 through 8 are generally consistent with vertical flow through the sediments, downward at Site 677 and upward at Site 678, at velocities of a few millimeters per year, as calculated by Langseth et al. (1988). The effect of vertical flow is especially clear for those elements that are less reactive in the sediments, such as Mg; their profiles at Sites 677 and 678 establish a range in concentration from that in bottom seawater to that in the upper basement formation water, within which all of the data from Site 501/504 fall. The surficial chemical gradients for these elements thus correlate directly with the surficial temperature gradients and heat flow.

Some of the chemical species that are reactive in the sediments, including Ca, sulfate, and K, also show this relationship, indicating that their profiles are heavily influenced by reaction in basement coupled with vertical flow. Only for those species that are most reactive in the sediments, including alkalinity, ammonium, Mn, Sr, Li, and Si, do the concentrations at Site 501/504 fall outside the range established by Sites 677 and 678. Even for some of these species, either Site 677 or 678 represents an extreme. At the warm Site 678, upflow brings the alkalinity value of the basement formation water closest to the seafloor. At the cool Site 677, downflow brings the concentration of Sr in bottom seawater closest to basement.

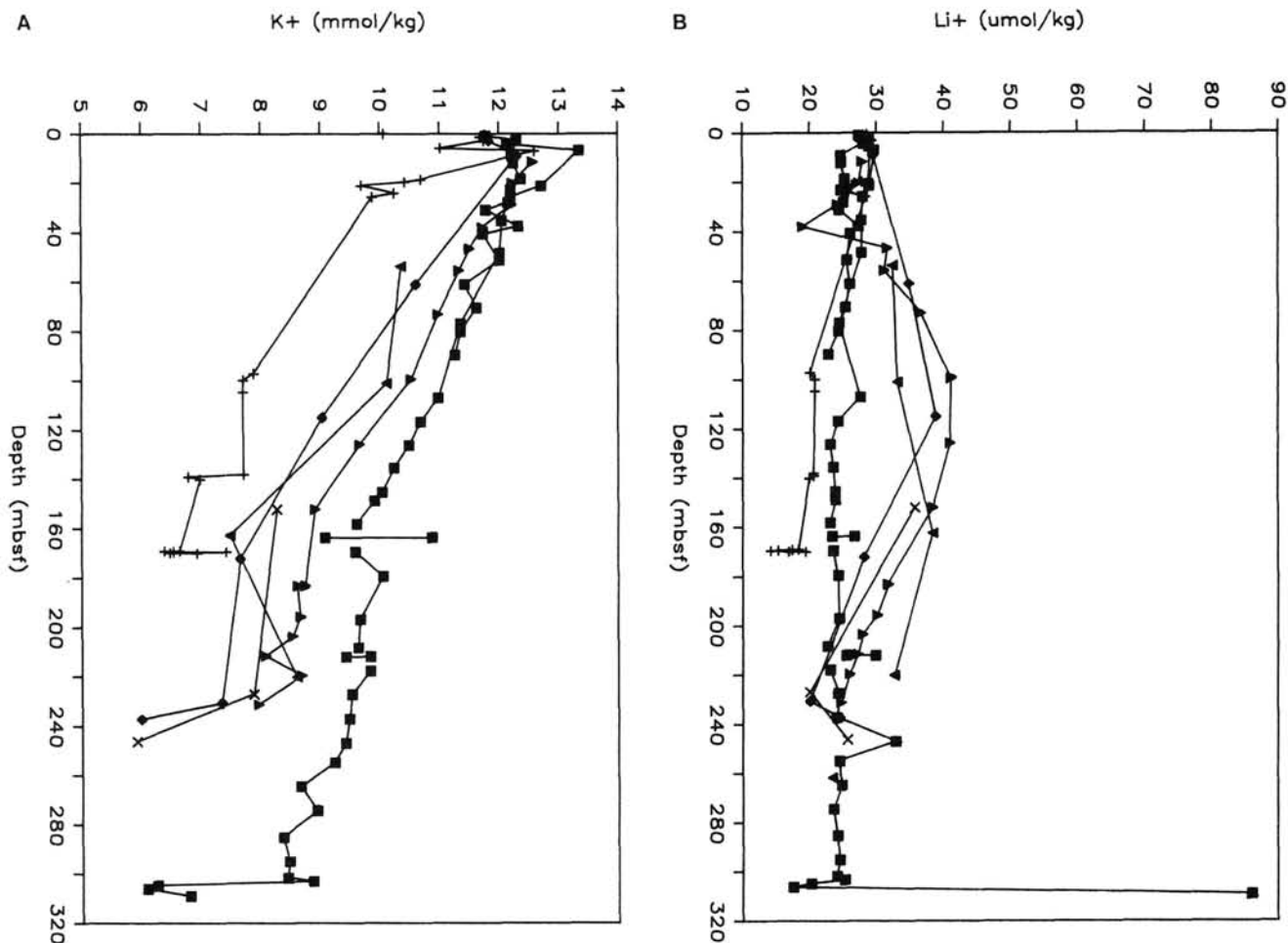


Figure 7. Concentrations of K^+ (A) and Li^+ (B) in sediment pore waters from Holes 677A, 677B, 678B, 501, 504, 504A, 504C, and 504B. Symbols are the same as in Figure 3.

Inferences from Chlorinity and Na

Two chemical species that appear to contradict these conclusions are chlorinity and Na, at least for Site 501/504 (Fig. 9). The holes at this site and at Site 677 exhibit a 2% to 3% maximum at 40 to 120 mbsf and a deeper minimum. McDuff (1985) noted that a 2% to 3% increase in chlorinity is a nearly ubiquitous feature of DSDP pore waters from rapidly deposited sediments. He attributed this increase to the higher chlorinity of seawater during the Pleistocene glaciations, as a result of increased ice volume. McDuff (1985) modeled the diffusion of the glacial-interglacial chlorinity signal downward into the sediments and found that a maximum should occur at about 30 mbsf, assuming that the chlorinity of basement formation water does not differ greatly from that of bottom water. He also demonstrated that this maximum is completely erased by upward flow at velocities in excess of 5 mm/yr.

The chlorinity profile at the warm Site 678 is entirely consistent with upward flow at a velocity of 1 to 2 mm/yr, as calculated by Langseth et al. (1988). It has a simple convex-upward shape and increases from the bottom-water value of 541 mmol/kg to the inferred value in the upper basement formation water of about 547 mmol/kg within the upper 20 m of the sediments (Fig. 9). The profiles for Na and Na/chlorinity (Fig. 10) share these features, as do the profiles for Ca, Mg, Ba, and alkalinity. With minor excursions resulting from rapid reaction in the sedi-

ments, so do the profiles for sulfate and Sr, and, with major excursions, K, ammonium, Si, and Mn.

The chlorinity profile at the cool Site 677 displays a maximum, with concentrations exceeding that of the inferred basement formation water, but consistent with that of Pleistocene bottom water as calculated by McDuff (1985). It is not obvious that this maximum has been displaced downward by downward flow. That such flow is occurring is more apparent from the profiles for Na and Na/chlorinity (Figs. 9 and 10). Na drops abruptly to the concentration inferred for the shallow basement formation water over the lower 35 m of sediment. Na/chlorinity does likewise, after staying nearly constant throughout the upper sediments at the value for bottom water. Given a diffusion coefficient of about $0.05 \text{ m}^2/\text{yr}$ in the deeper sediments, this large gradient implies a downward flow velocity of 1 to 2 mm/yr, similar to that for upward flow at Site 678. An alternative explanation for this gradient is that it results from variation in the diffusion coefficient, caused by diagenesis of the basal sediments. This alternative is addressed in the next section. More detailed modeling will be required to understand fully the chlorinity profile at this site, but it does not appear to preclude slow downward flow.

The profiles for chlorinity, Na, and Na/chlorinity at Site 501/504 resemble those at Site 677, except for the lower values below 180 mbsf at Site 501/504. The chlorinity maximum again exceeds the concentration inferred for formation water from the

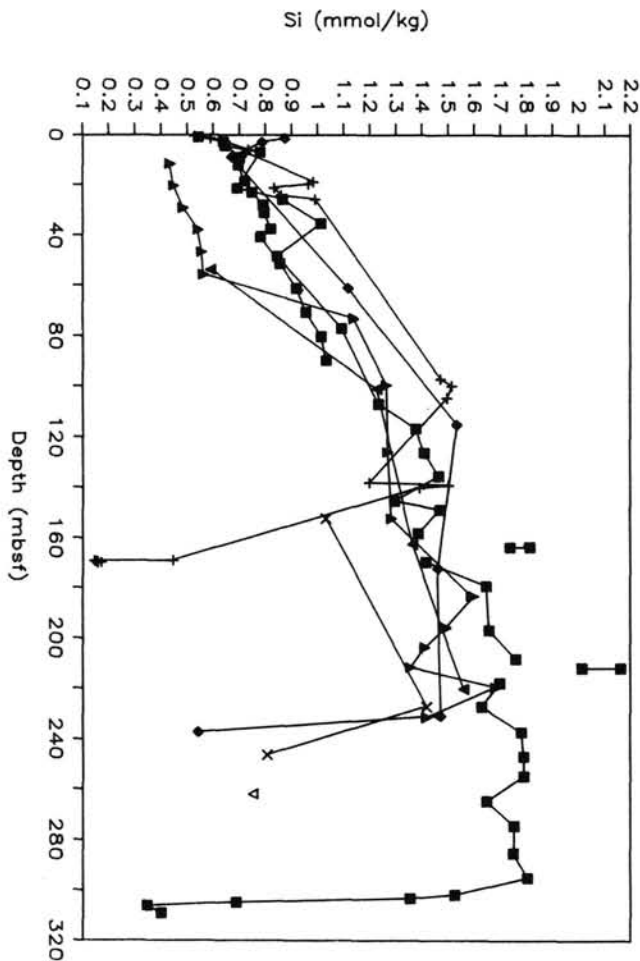


Figure 8. Concentration of Si in sediment pore waters from Holes 677A, 677B, 678B, 501, 504, 504A, 504B, and 504C. Symbols are the same as in Figure 3. The two *in-situ* samples from Hole 677A plot at higher concentrations than the squeezed samples from the same depths.

shallow basement. This rules out upward flow through the sediments at Site 501/504, except at velocities less than 5 mm/yr. In fact, the large size of the chlorinity maximum probably rules out flows faster than 1 mm/yr (McDuff, 1985). The higher-than-average heat flow at Site 501/504 rules out downward flow. It is likely, therefore, that the depth profiles for the various species at Site 501/504 result from a combination of reaction, diffusion, and possibly lateral flow.

Vertical Diffusion through the Sediments

The depth profiles for various species at Site 678 are relatively simple and consistent. They are convex upward, with a large gradient in the upper 20 m of the sediments and nearly constant values below that depth. They join the composition of bottom seawater at the top with the composition of shallow basement formation water at the base. This is the pattern shown by Ca, Mg, Na, chlorinity, Na/chlorinity, alkalinity, Ba, and Li. For those species that are more reactive in the sediments, there can be an extremum lying outside the range of composition between bottom water and formation water. This is the pattern shown by sulfate, Sr, ammonium, K, Si, and Mn. The depth profiles at the warm Site 678 are dominated by upward flow; any excursions in profile shape are readily explained by reaction in the sediments. The profiles at Sites 677 and 501/504 are more

complex. As a first step toward addressing these complexities, the effects of vertical diffusion at these sites can be modeled.

Modeling Vertical Diffusion

In order to quantify the role of diffusion it is necessary to know the variation in the sediment diffusion coefficient with depth and time. Only its present variation with depth is calculated here, as the timing of reheating and diagenesis of the sediments is not well known. Whereas Mottl et al. (1983) suggested on the basis of oxygen isotopic data that recrystallization of the basal sediments to chert and limestone at Site 501/504 occurred only in the past 200,000 yr, the heatflow data suggest a longer time period. Also, the effects of diagenesis with depth vary considerably among the three sites.

The diffusion coefficient for Ca in water is taken to be 0.063 m²/yr at 25°C. Its variation with temperature has been calculated from the relationship of McDuff and Gieskes (1976), $D^T = D^{T_0}[1 + 0.0345(T - T_0)]$. The temperature gradient used is that for Site 501/504 shown in Figure 2, as this gradient is better constrained than that at Site 677. The sediment diffusion coefficient has been calculated from the relationship $D_s = D/F$, where $F = \text{formation factor } R_s + pw/R_{\text{seawater}}$, the electrical resistivity of sediment plus pore water divided by the resistivity of the pore water alone, here approximated by seawater of similar chlorinity (Manheim and Waterman, 1974).

Formation factors measured for Sites 501/504, 505, 677, and 678 are shown in Figure 13, along with the curves for Sites 501/504 and 677 used in the calculations. The curve for Site 501/504 has two discontinuities that correspond to the two major diagenetic boundaries, from ooze to chalk and from chalk to interbedded limestone and chert. Because no resistivity measurements were made in the chert-limestone from this site, an average of the two measurements from this zone at Site 677 was used, as shown. Site 677 has only one discontinuity in the resistivity data, at the base near the boundary between chalk and cherty limestone.

The resulting sediment diffusion coefficients show corresponding discontinuities with depth (Fig. 14). Note that for Site 501/504, D_s increases with depth following the abrupt decreases at the diagenetic boundaries, due to the continued increase in temperature with depth.

These present-day values for D_s were assumed to be time-invariant and were used to calculate the development of depth profiles for Ca in the sediment pore waters with time, neglecting reaction, convection, and sedimentation. Besides a diagenetically altered sediment section, the initial and constant conditions included an upper boundary at the seafloor with 10 mmol/kg Ca and a lower boundary at the basement interface with 55 mmol/kg Ca; that is, reaction in basement had already produced a formation water similar to that inferred for the present, which remained constant throughout the time period covered by the calculations. Based on measurements from Sites 677 and 501/504, the porosity of the sediments was assumed to vary linearly from 80% at the seafloor to 65% at the basement interface. The sediment section was divided into 10-m-thick boxes and Fick's second law of diffusion was solved iteratively for each box for each time step. Time steps were 10 yr for the first 100 yr, 50 yr from 100 to 2500 yr, and 500 yr from 2500 yr to 1.5 m.y.

Results in the Absence of Diagenesis

The results of these calculations for a 275-m-thick sediment section with no diagenetic alteration are shown in Figure 15. The formation factor used is the regression line in Figure 13, with no discontinuities. The shape of the depth profile changes only slowly after about 1 m.y. The approach to steady state is shown in Figure 16.

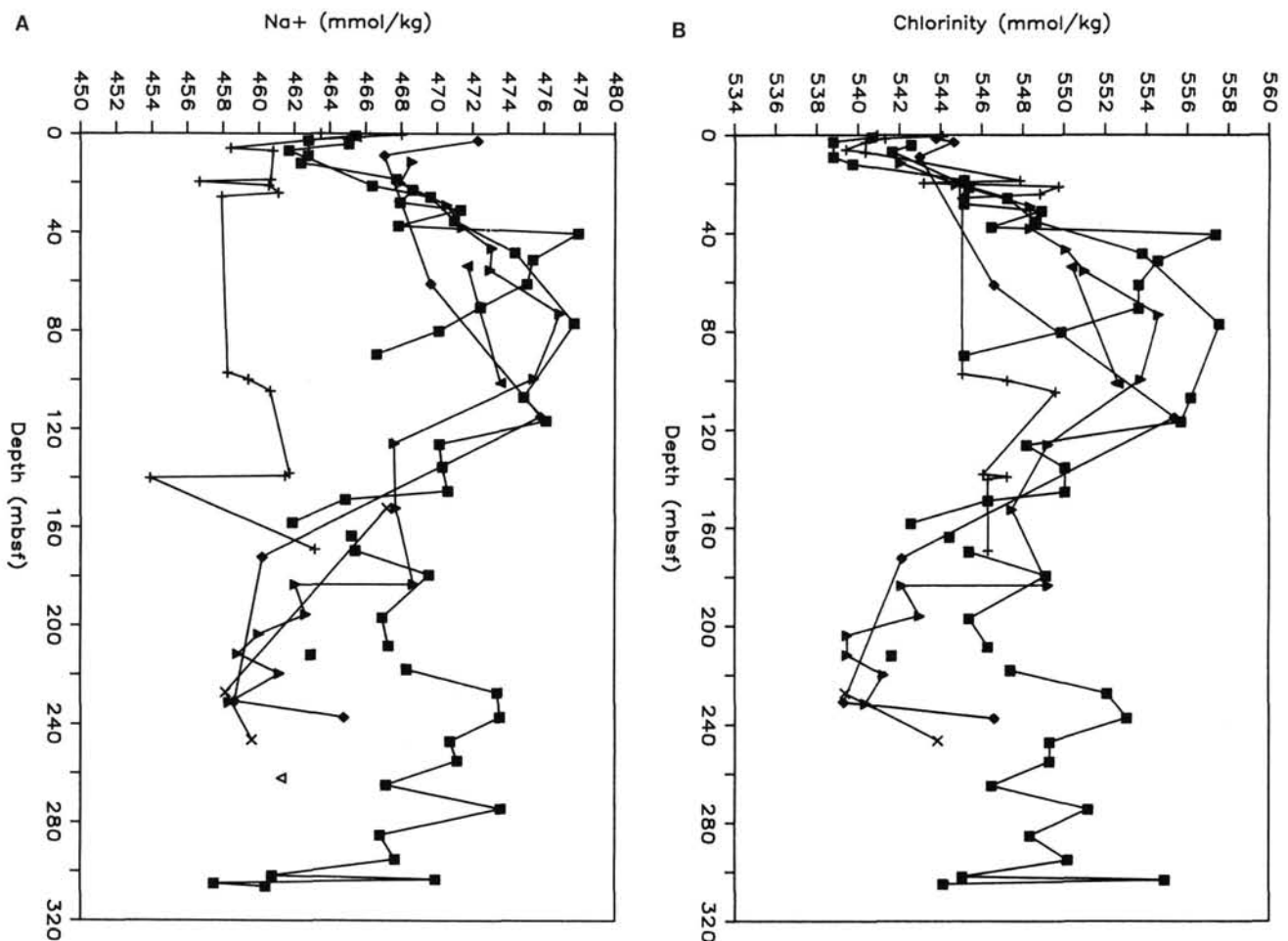


Figure 9. Concentrations of Na^+ (A) and chlorinity (B) in sediment pore waters from Holes 677A, 677B, 678B, 501, 504, 504A, 504C, and 504B. Symbols are the same as in Figure 3.

The diagenesis-free profile is compared with calculated profiles for Sites 677 and 501/504 in Figure 17, for an elapsed time of 1.5 m.y. and adjusted to a constant sediment thickness of 275 m. Note that diagenesis of the basal sediments to cherty limestone as at Site 677 has produced only a small deviation from the diagenesis-free profile, in spite of a tripling in the formation factor near basement. The profile for Site 501/504 deviates significantly from the diagenesis-free profile, showing two additional bends and a large offset to lower concentrations over most of the depth range.

Results for Site 677

The measured Ca profile for Site 677 is compared with the calculated profiles for elapsed times from 10,000 yr to 1.4 m.y. in Figure 18. The calculated steady-state gradient near basement is much smaller than the gradient observed in the basal sediments, even when the lowermost measurement is discounted as a sampling artifact. The observed gradient is comparable to that calculated for an elapsed time of less than 10,000 yr. If the observed gradient is due primarily to diffusion through a diagenetically altered basal layer rather than to downward flow, then the basement formation water must have become highly enriched in Ca only recently, within the past 10,000 yr.

This possibility can be ruled out by the profiles from the nearby sites. Basement formation water at Site 678 has similarly enhanced Ca, which has propagated upward through at least the lower 150 m of sediments there. At the inferred upflow veloci-

ties of 1 to 2 mm/yr, this would have required at least 75,000 to 150,000 yr, indicating that the basement formation water at Site 678 has been enriched in Ca for at least that long. If the enhanced Ca propagated upward by diffusion, as may be the case at Site 501/504, on the order of 1 m.y. would be required, as noted by Mottl et al. (1983), for the oxygen isotopic profiles there. Sites 678 and 501/504 are only 2.0 and 2.6 km distant from Site 677, respectively (Fig. 1). At the lateral flow velocities of 10 to 30 cm/yr inferred by Langseth et al. (1988) for water in the shallow basement, no more than 20,000 yr would be required for the Ca-rich waters to arrive at Site 677.

The large gradient in sediment pore-water composition near basement at Site 677 therefore cannot result from diffusion alone. As discussed in the previous section, it almost certainly results from slow downward flow. The other gradient in the depth profile, which doubles the Ca concentration between 110 and 160 mbsf, must result from reaction and/or lateral diffusion or convection, as discussed in the next section.

Results for Site 501/504

The measured Ca profiles for Holes 501 and 504 are compared with the calculated profiles for elapsed times from 10,000 yr to 1.4 m.y. in Figure 19. Over most of the depth range, the calculated steady-state profile falls between the measured profiles for the two holes, which were drilled only about 260 m apart. Both the measured and calculated curves are S-shaped, but they are out of phase with one another, causing them to suc-

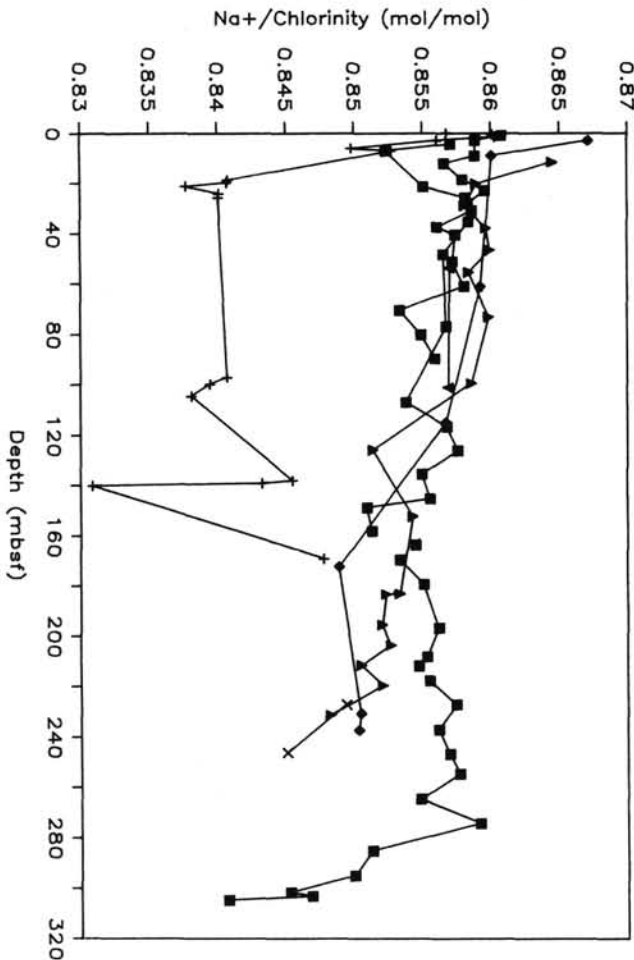


Figure 10. Ratio of Na^+ to chlorinity vs. depth in sediment pore waters from Holes 677A, 677B, 678B, 501, 504, 504A, and 504C. Symbols are the same as in Figure 3.

cessively diverge and converge with depth. Clearly the S shape of the measured profiles does not result from changes in vertical diffusion at the diagenetic boundaries, unless these boundaries are migrating much faster than the diffusive flux itself. This is highly unlikely. As the profiles at Site 501/504 cannot be produced by either vertical convection or vertical diffusion, alone or in combination, they must result from reaction and/or lateral diffusion or convection.

Lateral Diffusion and Convection through the Sediments

Two characteristics of the depth profiles that cannot be explained by the processes discussed so far are the changes at 110 to 160 mbsf at Site 677 and the S-shaped profiles at Site 501/504. At Site 677, Ca increases from 10 to 20 mmol/kg between 107 and 164 mbsf whereas Mg decreases by an equivalent amount. The Sr profile parallels that of Ca, although it is more subdued. Na, K, sulfate, Mn, and possibly chlorinity and Na/chlorinity exhibit a generally sharp break in slope within this interval, at about 160 mbsf. The difference between the sulfate loss and the alkalinity gain goes from negative to positive (Fig. 11). Alkalinity, ammonium, Si, Li, and Ba show no obvious change. At Site 501/504, the depth profiles for Ca, Mg, and Sr change from nearly linear in Hole 504C to more convex-upward through Holes 504 and 501, as the depth to the first large Ca increase becomes shallower.

These two characteristics at Sites 677 and 501/504 may be related, as suggested by the gradual change in the shape of the depth profiles which is evident in Figure 3. In any case, these features cannot easily be explained by vertical convection and diffusion.

The basement at Site 678 is at 172 mbsf, close to the depth at which the changes in slope occur in the profiles at Site 677. Site 678 is located on a small hill; this and the shallow depth to basement suggest that it overlies an uplifted fault block, which probably has acted in some way to localize the upward flow through the sediments. The largest warm spot in the survey area, on a ridge about 3 km southwest of Site 677 (Fig. 1), also has a substantially thinner than average sediment cover of less than 200–250 m (Langseth et al., 1988; Shipboard Scientific Party, 1988b). The depth to the seafloor and basement at the drill sites is shown in Figure 20, along with that estimated for the warm spot southwest of Site 677. As can be seen, Site 677 lies midway between two sites of especially shallow basement with associated warm spots and upward flow through the sediments. Site 501/504, although in a different direction from the Site 678 warm spot (northeast), lies at a distance that is intermediate between Sites 677 and 678, in keeping with its intermediate pore-water chemical gradients.

It is likely at these sites of abnormally shallow basement, with their overlying zones of upflow, that the chemical signal from basement formation water propagates laterally as well as vertically through the sediments. Lateral propagation by diffusion would be inevitable in this situation, and may be accompanied by lateral flow as well. Site 678 is 1.3 km from Site 501/504 and 2.0 km from Site 677. Diffusion alone would require more than a million years for the signal to travel this far. More detailed two-dimensional modeling will be required to clarify the role of lateral diffusion and convection at these sites.

SUMMARY AND CONCLUSIONS

Drilling at ODP Sites 677 and 678 was extremely successful in testing the hypotheses of hydrothermal circulation formulated after several site surveys and DSDP Site 501/504. Sediment pore-water profiles confirm that warm water from basement is upwelling through the sediments at Site 678 at velocities of 1 to 2 mm/yr. The upflow is apparently localized within a broader band of high heat flow by anomalously shallow basement, which probably represents an uplifted fault block. A complementary downflow of bottom seawater occurs at Site 677, within a band of low heat flow 2 km to the south, at comparable velocities. The composition of the basal sediment pore water at the two sites and at Site 501/504 is virtually identical, in spite of large differences in heat flow, sediment thickness, and the shapes of the sediment pore-water profiles with depth.

Based on eight drill holes at three sites, 25 piston cores, and 300 heatflow measurements over a 100-km² survey area, it is now possible to present a more complete picture of hydrothermal circulation for this area on the southern flank of the Costa Rica Rift than for virtually any other place on a mid-ocean ridge flank. The picture that emerges is of broad upwelling and downwelling of heated seawater through basement, on a scale of several kilometers and driven by thermal convection. At the prevailing temperatures in basement of 60°C and at higher temperatures, this heated seawater has reacted extensively with the basement basalts. The resulting formation water near the top of basement is about 85% depleted in Mg along with Na, K, sulfate, and alkalinity. It is enriched relative to seawater in Ca, Si, and chlorinity. Its composition is uniform laterally over distances of several kilometers, from zones of upwelling to zones of downwelling, from high heat flow to low, from thin sediment to thick, from basement high to low. This uniformity presumably results from homogenization by hydrothermal circulation in basement.

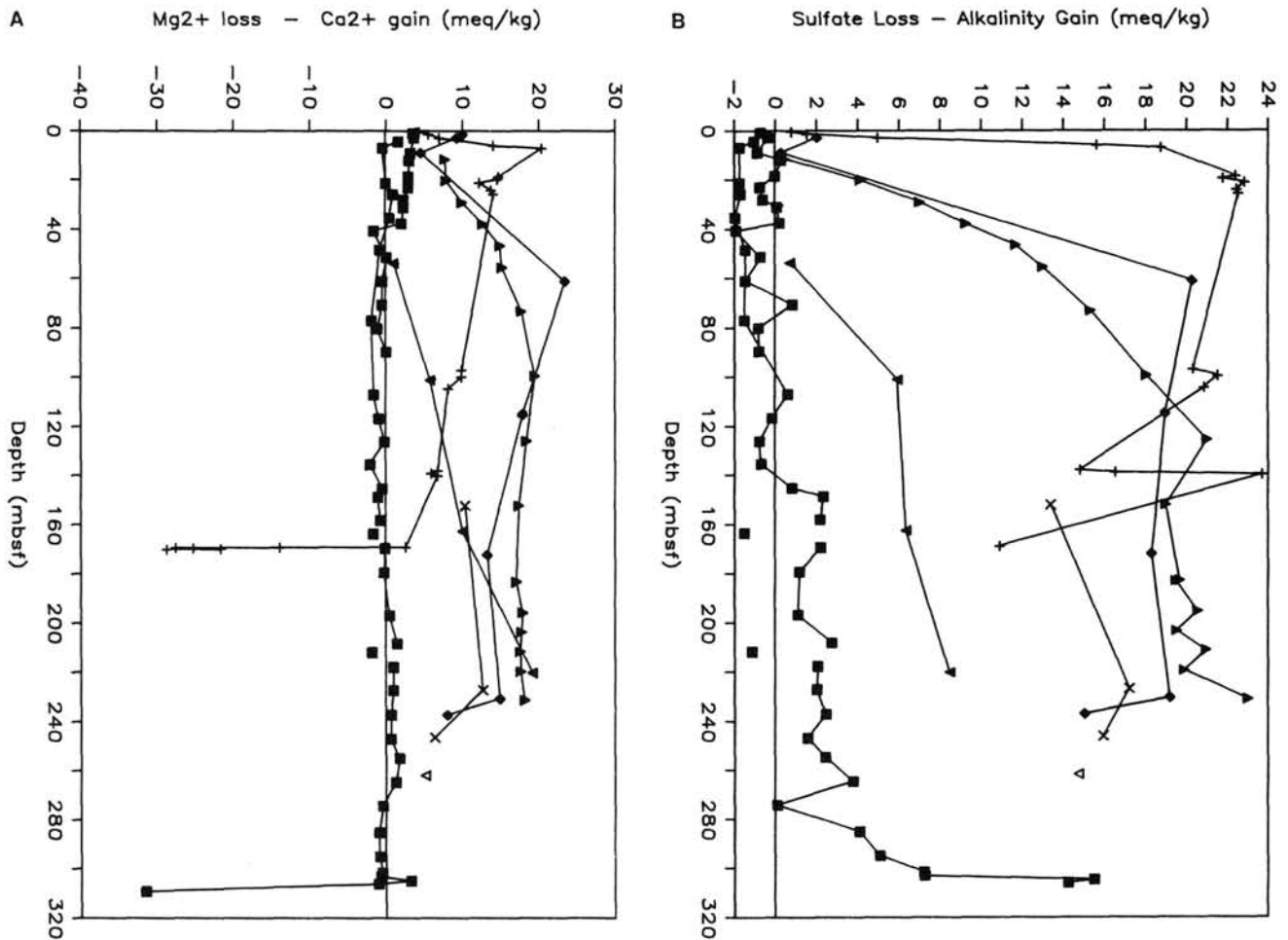


Figure 11. The difference between the Mg^{2+} loss and the Ca^{2+} gain (A) and between the sulfate loss and the alkalinity gain (B) relative to bottom seawater in sediment pore waters from Holes 677A, 677B, 678B, 501, 504, 504A, 504C, and 504B. Symbols are the same as in Figure 3.

Overlying the broad regions of upwelling in basement are smaller areas of upwelling through the sediments. The upwelling occurs at rates too slow to be thermally significant, except for local redistribution of heat flow: the surficial temperature gradients are linear, and heat loss from the area as a whole occurs overwhelmingly by conduction rather than advection. The warm spots created by upwelling appear to be localized in areas of abnormally thin sediment cover, possibly by structural uplifts in basement. They have persisted within areas only a few hundred to a few thousand meters across for a long time, on the order of a million years. They are surrounded by diffusive and possibly convective haloes, which give rise to lateral gradients in sediment pore-water composition surrounding the warm spots.

Overlying the broad regions of downwelling in basement are areas of downwelling through the sediments, such as at Site 677. As this site is the only one of its kind drilled so far, however, and because downwelling cannot be detected within the surficial sediments accessible to piston coring, little is known about the distribution of this downwelling. In addition, its effect on the thermal gradient in the sediments is unknown, as no reliable temperature measurements were made below 93 mbsf at this site.

Among mid-ocean ridge flanks, the Costa Rica Rift represents an extreme case: its smooth basement and high sedimentation rate seal the seafloor to advective heat loss there at a younger age than anywhere else, less than 6 m.y. (Anderson et al., 1977). This causes the upper basement to reheat to an unusual degree, speeding reaction between the circulating seawater and

the basement rocks. The amount of compositional change observed at these drill sites therefore probably represents an upper limit for formation water on a mid-ocean ridge flank of this age. The significance of these processes for chemical fluxes between oceans and the oceanic crust depends upon the maximum flow velocities, which have probably not yet been sampled, and the total area of seafloor that is affected. Much more work is required on other mid-ocean ridge flanks before these variables can be assessed.

ACKNOWLEDGMENTS

Thanks are due to J. M. Gieskes, F. L. Sayles, and R. J. Taylor for their constructive comments on an earlier draft of this manuscript. Formation factor data for Holes 677A and 678B were kindly provided by Mike Lovell. This work was supported by the National Science Foundation through grant OCE 86-08261 to MJM and through the Ocean Drilling Program. This is contribution number 2171 from the Hawaii Institute of Geophysics.

REFERENCES

- Anderson, R. N., Langseth, M. G., and Sclater, J. G., 1977. The mechanism of heat transfer through the floor or the Indian Ocean. *J. Geophys. Res.*, 82:3391-3409.
- Gieskes, J., 1983. The chemistry of interstitial waters of deep sea sediments, interpretation of Deep Sea Drilling data. In Riley, J. P., and Skirrow, G. (Eds.), *Chemical Oceanography* (vol. 8): New York (Academic Press), 221-269.
- Langseth, M. G., Mottl, M. J., Hobart, M. A., and Fisher, A., 1988. The distribution of geothermal and geochemical gradients near Site

501/504: implications for hydrothermal circulation in the oceanic crust. *In* Becker, K., Sakai, H., et al., *Proc. ODP, Init. Repts.*, 111: College Station, TX (Ocean Drilling Program), 23-32.

Manheim, F. T., and Waterman, L. S., 1974. Diffusimetry (diffusion constant estimation) on sediment cores by resistivity probe. *In* von der Borch, C. C., Sclater, J. G., et al., *Init. Repts. DSDP*, 22: Washington (U.S. Govt. Printing Office), 663-670.

McDuff, R. E., 1985. The chemistry of interstitial waters, Deep Sea Drilling Project Leg 86. *In* Heath, G. R., Burckle, L. H., et al., *Init. Repts. DSDP*, 86: Washington (U.S. Govt. Printing Office), 675-687.

McDuff, R. E., and Gieskes, J. M., 1976. Calcium and magnesium profiles in DSDP interstitial waters: diffusion or reaction? *Earth Planet. Sci. Lett.*, 33:1-10.

Mottl, M. J., Druffel, E.R.M., Hart, S. R., Lawrence, J. R., and Saltzman, E. S., 1985. Chemistry of hot waters sampled from basaltic basement in Hole 504B, DSDP Leg 83, Costa Rica Rift. *In* Anderson, R. N., Honnorez, J., Becker, K., et al., *Init. Repts. DSDP*, 83: Washington (U.S. Govt. Printing Office), 315-328.

Mottl, M. J., and Gieskes, J. M., in press. Chemistry of waters sampled from oceanic basement boreholes, 1979-1988. *J. Geophys. Res.*

Mottl, M. J., Lawrence, J. R., and Keigwin, L. D., 1983. Elemental and stable-isotope composition of pore waters and carbonate sediments from Deep Sea Drilling Project Sites 501/504 and 505. *In* Cann, J. R., Langseth, M. G., et al., *Init. Repts. DSDP*, 69: Washington (U.S. Govt. Printing Office), 461-473.

Seyfried, W. E., Jr., and Bischoff, J. L., 1979. Low temperature basalt alteration by seawater: an experimental study at 70°C and 150°C. *Geochim. Cosmochim. Acta*, 43:1937-1947.

Seyfried, W. E., Jr., and Mottl, M. J., 1982. Hydrothermal alteration of basalt by seawater under seawater-dominated conditions. *Geochim. Cosmochim. Acta*, 46:985-1002.

Shipboard Scientific Party, 1988a. Site 504: Costa Rica Rift. *In* Becker, K., Sakai, H., et al., *Proc. ODP, Init. Repts.*, 111: College Station, TX (Ocean Drilling Program), 35-251.

_____, 1988b. Sites 677 and 678. *In* Becker, K., Sakai, H., et al., *Proc. ODP, Init. Repts.*, 111: College Station, TX (Ocean Drilling Program), 253-295.

Date of initial receipt: 14 November 1988

Date of acceptance: 14 April 1989

Ms 111B-125

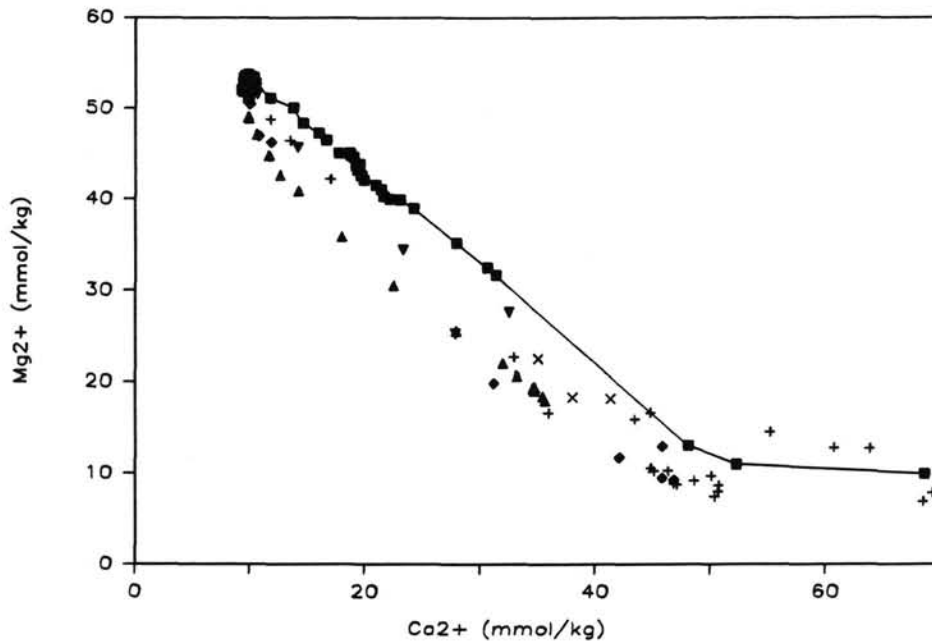


Figure 12. Concentration of Ca^{2+} vs. Mg^{2+} in sediment pore waters from Holes 677A, 677B, 678B, 501, 504, 504A, 504C, and 504B. Symbols are the same as in Figure 3.

Table 2. Composition of basal sediment pore water from Sites 501/504, 677, and 678, compared with waters sampled from the basement section of Hole 504B.

	Depth (mbsf)	Temp. (°C)	Chlorinity (mmol/kg)	Sulfate (mmol/kg)	Alkalinity (meq/kg)	Na ⁺ (mmol/kg)	K ⁺ (mmol/kg)	Ca ²⁺ (mmol/kg)	Mg ²⁺ (mmol/kg)	Si (mmol/kg)	Na/Cl (mol/mol)
Bottom seawater	0	2	540.9	27.9	2.44	463.5	10.1	10.2	52.6	-0.16	0.8568
Basal sediment pore water	~300	~60	547	18.5	0.5	459	6.5	52	8	-0.30	0.8391
^a Basement borehole waters, Hole 504B											
Leg 111 RFT-1	466	81	532.3	26.9	2.09	454.5	9.9	13.6	48.4	0.24	0.8538
Leg 83 PA-1	478.5	81	549.5	24.6	2.50	456.3	8.6	28.5	39.6	0.76	0.8304
Leg 111 KUS-1	631	101	540.6	24.0	1.38	449.4	9.6	21.0	44.4	0.52	0.8313
Leg 111 RFT-2	766	115	537.0	21.6	1.54	444.1	8.8	24.5	39.9	1.10	0.8270
Leg 83 PA-2	792.5	116	549.9	14.7		435.2	6.4	47.8	20.1	2.20	0.7914
Leg 111 RFT-3	1236	146	540.8	-0.5	0.97	398.8	7.3	45.8	21.5	2.62	0.7374

^a Leg 83 data are from Mottl et al. (1985) and Mottl and Gieskes (1989); Leg 111 data are from Shipboard Scientific Party (1988a).

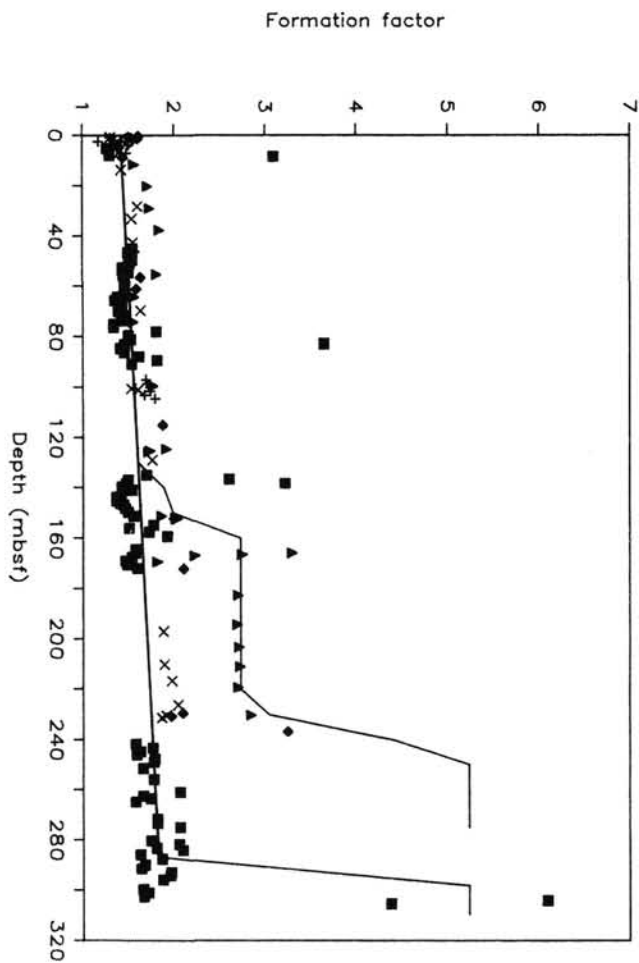


Figure 13. Formation factors measured on sediment cores from Holes 677A (squares), 678B (crosses), 501 (diamonds), 504 (triangles), and 505 (X's). The least-squares regression line from 0 to 285 mbsf has the equation $F = 0.001414d + 1.42632$.

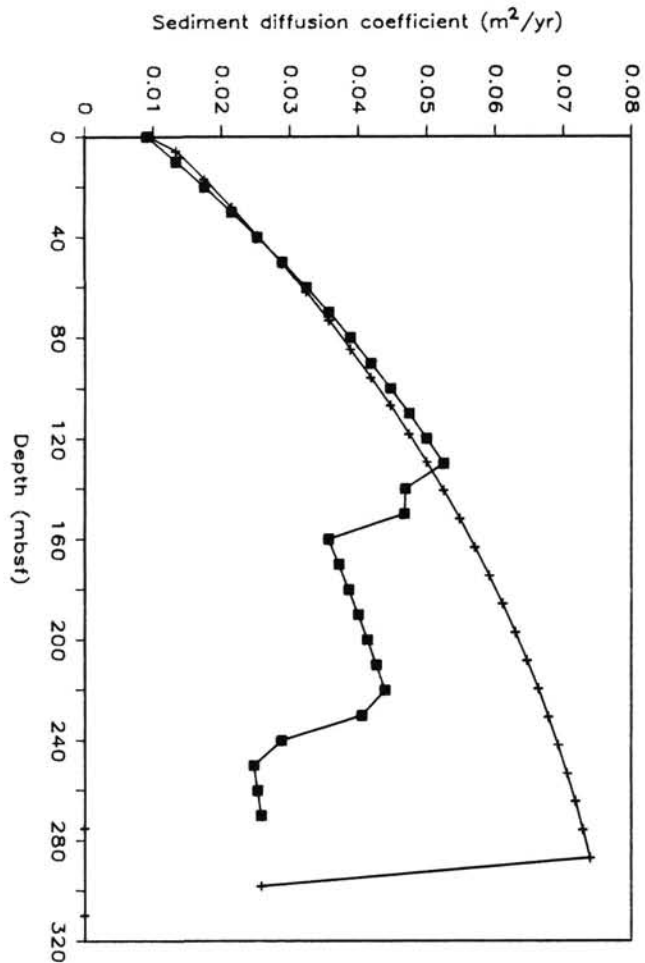


Figure 14. Sediment diffusion coefficient vs. depth calculated for Sites 501/504 (squares) and 677 (crosses).

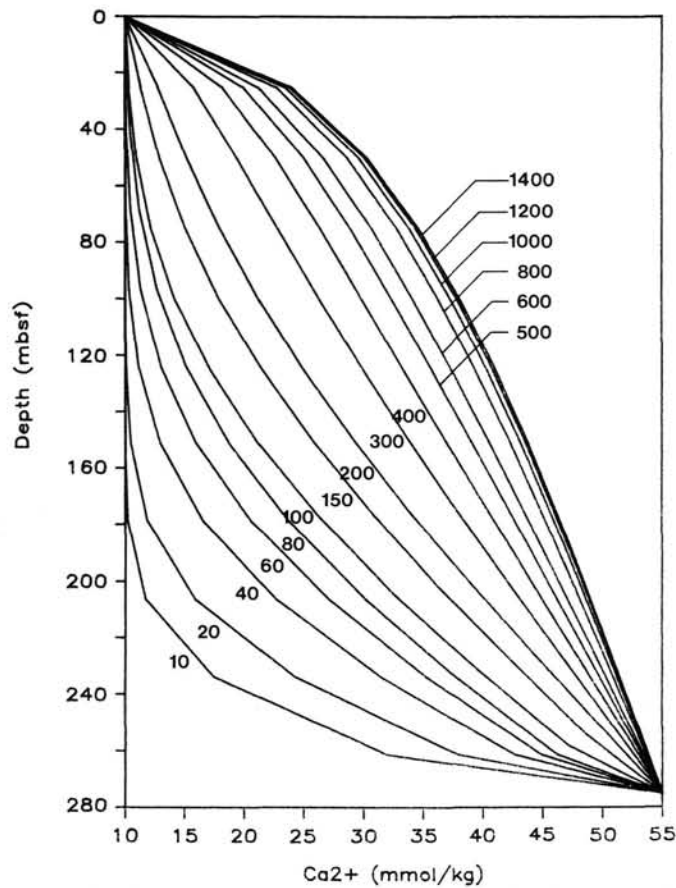


Figure 15. Calculated evolution of the depth profile for Ca in the sediment pore waters over a period of 1.4 m.y., resulting from one-dimensional diffusion upward from basement in the absence of diagenesis. Curve labels for elapsed times are in 1000-yr units of 10, 20, 40, 60, 80, 100, 150, 200, 300, 400, 500, 600, 800, 1000, 1200, and 1400. The formation factor used is the regression line in Figure 13.

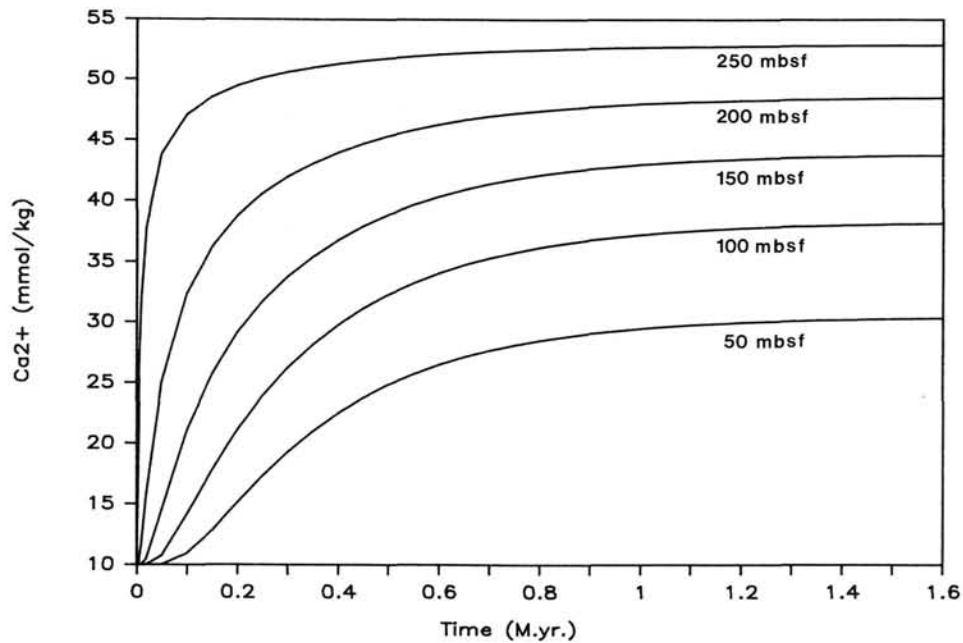


Figure 16. Change in sediment pore-water composition with time due to diffusion, at five depths in a 275-m-thick sediment section, calculated according to the diagenesis-free model in Figure 15.

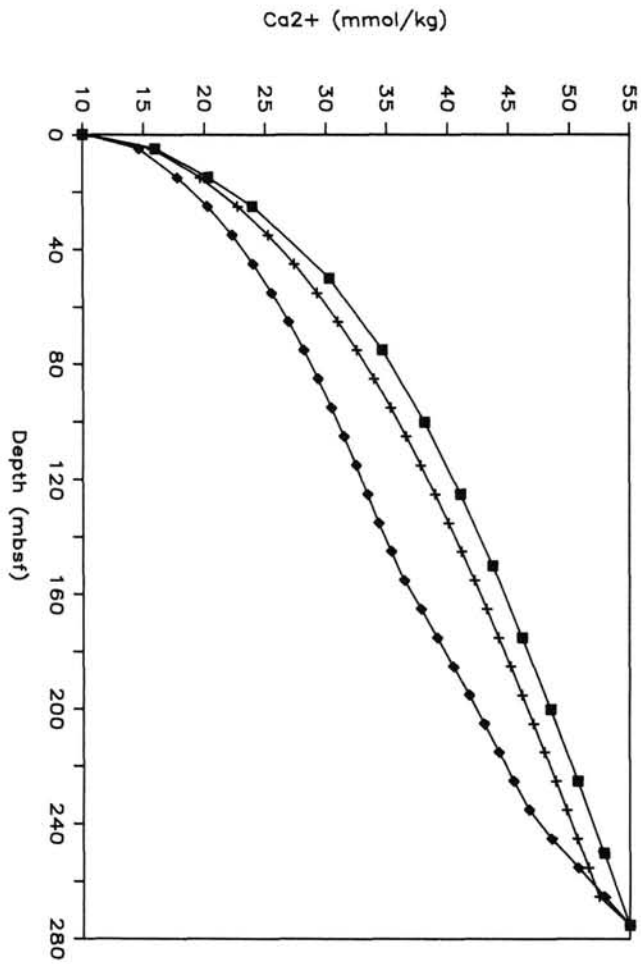


Figure 17. Comparison of the calculated diffusive sediment pore-water profiles after 1.5 m.y. for three cases of varying formation factor (Fig. 13) and sediment diffusion coefficient (Fig. 14) vs. depth: no diagenesis (squares), basal diagenesis as at Site 677 (crosses), and two diagenetic boundaries as at Site 501/504 (diamonds).

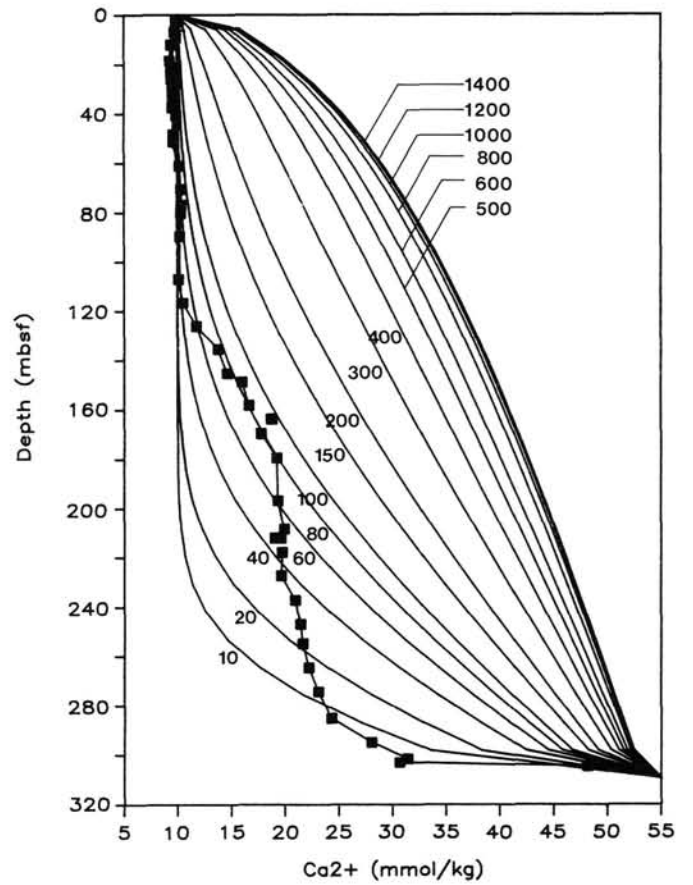


Figure 18. Comparison between the measured profile for Ca in the sediment pore waters at Site 677 (squares) and the calculated diffusive profiles for elapsed times of 10,000 yr to 1.4 m.y. The lowermost sample was deleted because it is believed to be affected by sampling artifacts.

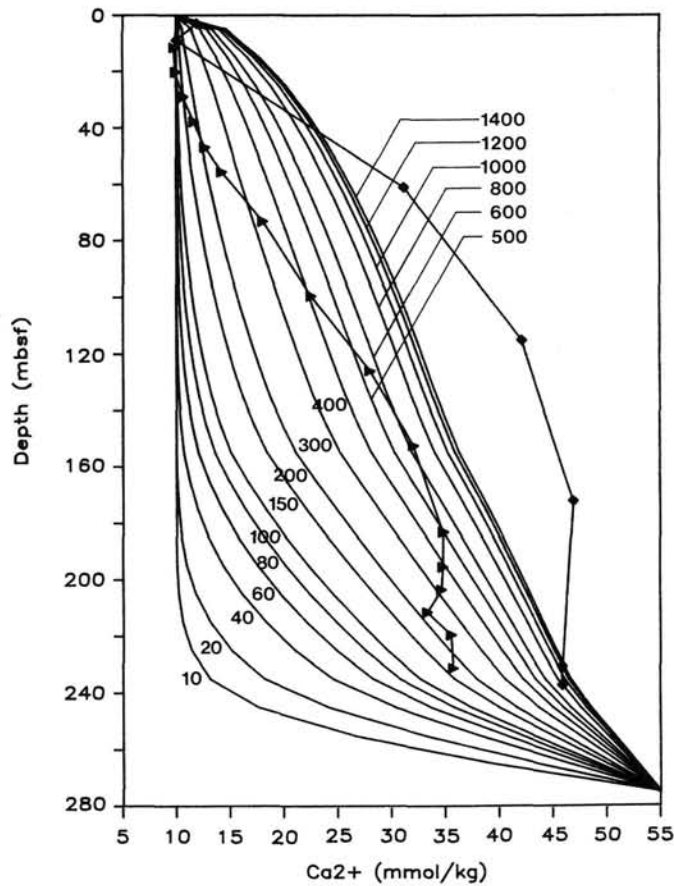


Figure 19. Comparison of the measured profiles for Ca in the sediment pore waters in Holes 501 (diamonds) and 504 (triangles) with the calculated diffusive profiles for elapsed times of 10,000 yr to 1.4 m.y.

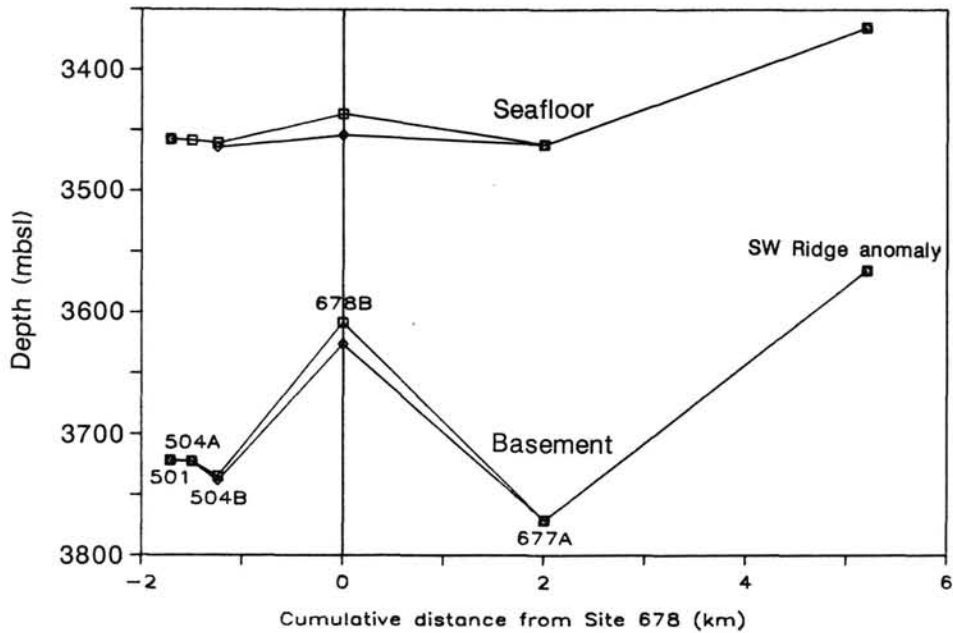


Figure 20. Depth to the seafloor and basement, as measured for five drill holes and estimated from seismic-reflection profiling for the heatflow high on the ridge southwest of Site 677.